ACKNOWLEDGMENTS

This work was supported in part by Health and Labor Sciences Research Grants (Research on Pharmaceutical and Medical Safety), Ministry of Health, Labor and Welfare, Japan.

REFERENCES

1. Chang, T.M.S. (2000). Is there a need for blood substitutes in the new millennium and what should we expect in the way of safety and efficacy ? *Art. Cells, Blood Subs., and Immob. Biotech.* **28**: v–xi.
2. Johnson, J.L., Moore, E.E., Offner, P.J., Haenel, J.B., Hides, G.A., Tamura, D.Y. (1998). Resuscitation of the injured patient with polymerized stroma-free hemoglobin does not produce systemic or pulmonary hypertension. *Am. J. Surg.* **176**: 612–617.
3. Mullon, J., Giacoppe, G., Clagett, C., McCune, D., Dillard, T. (2000). Transfusions of polymerized bovine hemoglobin in a patient with severe autoimmune hemolytic anemia. *N. Engl. J. Med.* **342**: 1638–1643.
4. Carmichael, F.J., Ali, A.C., Campbell, J.A., Langlois, S.F., Biro, G.P., Willan, A.R., Pierce, C.H., Greenburg, A.G. (2000). A phase I study of oxidized raffinose cross-linked human hemoglobin. *Crit. Care Med.* **28**: 2283–2292.
5. Sakai, H., Tomiyama, K.I., Sou, K., Takeoka, S., Tsuchida, E. (2000). Poly (ethylene glycol)-conjugation and deoxygenation enable long-term preservation of hemoglobin-vesicles as oxygen carriers in a liquid state. *Bioconjug. Chem.* **11**: 425–432.
6. Tsuchida, E., Takeoka, S. (1995). Stabilized hemoglobin vesicles, in *Artificial Red Cells: Materials, Performances and Clinical Study as Blood Substitutes*, E. Tsuchida, Ed., John Wiley and Sons: Chichester, pp. 35–64.
7. Izumi, Y., Sakai, H., Kose, T., Hamada, K., Takeoka, S., Yoshizu, A., Horinouchi, H., Kato, R., Nishide, H., Tsuchida, E., Kobayashi, K. (1997). Evaluation of the capabilities of a hemoglobin vesicle as an artificial oxygen carrier in a rat exchange transfusion model. *ASAIO J.* **43**: 289–297.
8. Izumi, Y., Sakai, H., Hamada, K., Takeoka, S., Yamahata, T., Kato, R., Nishide, H., Tsuchida, E., Kobayashi, K. (1996). Physiologic responses to exchange transfusion with hemoglobin vesicles as an artificial oxygen carrier in anesthetized rats: changes in mean arterial pressure and renal cortical tissue oxygen tension. *Crit. Care Med.* **24**: 1869–1873.
9. Sakai, H., Takeoka, S., Park, S.I., Kose, T., Nishide, H., Izumi, Y., Yoshizu, A., Kobayashi, K., Tsuchida, E. (1997). Surface modification of hemoglobin vesicles with poly(ethylene glycol) and effects on aggregation, viscosity, and blood flow during 90% exchange transfusion in anesthetized rats. *Bioconjug. Chem.* **8**: 23–30.
10. Sakai, H., Horinouchi, H., Tomiyama, K., Ikeda, E., Takeoka, S., Kobayashi, K., Tsuchida, E. (2001). Hemoglobin-vesicles as oxygen carriers: influence on phagocytic activity and histopathological changes in reticuloendothelial system. *Am. J. Pathol.* **159**: 1079–1088.

11. Sakai, H., Takeoka, S., Wettstein, R., Tsai, A.G., Intaglietta, M., Tsuchida, E. (2002). Systemic and microvascular responses to hemorrhagic shock and resuscitation with Hb vesicles. *Am. J. Physiol. Heart Circ. Physiol.* **283**: H1191–1199.
12. Rand, M.L., Leung, R., Packham, M.A. (2003). Platelet function assays. *Transfus Apheresis Sci.* **28**: 307–317.
13. Klinger, M.H. (1997). Platelets and inflammation. *Anat. Embryol. (Berl).* **196**: 1–11.
14. Sou, K., Naito, Y., Endo, T., Takeoka, S., Tsuchida, E. (2003). Effective encapsulation of proteins into size-controlled phospholipid vesicles using freeze-thawing and extrusion. *Biotechnol. Prog.* **19**: 1547–1552.
15. Hagberg, I.A., Lyberg, T. (2000). Blood platelet activation evaluated by flow cytometry: optimised methods for clinical studies. *Platelets* **11**: 137–150.
16. Kohmura, C., Hayashi, Y., Ikeda, H. (1999). Detection of activated platelets by flow cytometry. *Rinsho Byori* **47**: 447–452.
17. Santos, M.T., Valles, J., Marcus, A.J., Safier, L.B., Broekman, M.J., Islam, N., Ullman, H.L., Eiroa, A.M., Aznar, J. (1991). Enhancement of platelet reactivity and modulation of eicosanoid production by intact erythrocytes. A new approach to platelet activation and recruitment. *J. Clin. Invest.* **87**: 571–580.
18. Hynes, R.O. (1992). Integrins: versatility, modulation, and signaling in cell adhesion. *Cell* **69**: 11–25.
19. Shattil, S.J., Hoxie, J.A., Cunningham, M., Brass, L.F. (1985). Changes in the platelet membrane glycoprotein IIb: IIIa complex during platelet activation. *J. Biol. Chem.* **260**: 11107–11114.
20. Samuelsson, B., Goldyne, M., Granstrom, E., Hamberg, M., Hammarstrom, S., Malmsten, C. (1978). Prostaglandins and thromboxanes. *Annu. Rev. Biochem.* **47**: 997–1029.
21. Ruggeri, Z.M. (2002). Platelets in atherothrombosis. *Nat. Med.* **8**: 1227–1234.
22. Merten, M., Thiagarajan, P. (2000). P-selectin expression on platelets determines size and stability of platelet aggregates. *Circulation* **102**: 1931–1936.
23. Stenberg, P.E., McEver, R.P., Shuman, M.A., Jacques, Y.V., Bainton, D.F. (1985). A platelet alpha-granule membrane protein (GMP-140) is expressed on the plasma membrane after activation. *J. Cell. Biol.* **101**: 880–886.
24. Palabrica, T., Lobb, R., Furie, B.C., Aronovitz, M., Benjamin, C., Hsu, Y.M., Sajer, S.A., Furie, B. (1992). Leukocyte accumulation promoting fibrin deposition is mediated in vivo by P-selectin on adherent platelets. *Nature* **359**: 848–851.
25. Schmidtke, D.W., Diamond, S.L. (2000). Direct observation of membrane tethers formed during neutrophil attachment to platelets or P-selectin under physiological flow. *J. Cell. Biol.* **149**: 719–730.
26. Baggiolini, M., Dahinden, C.A. (1994). CC chemokines in allergic inflammation. *Immunol. Today* **15**: 127–133.
27. Brandt, E., Ludwig, A., Petersen, F., Flad, H.D. (2000). Platelet-derived CXC chemokines: old players in new games. *Immunol. Rev.* **177**: 204–216.

Human Serum Albumin Bearing Covalently Attached Iron(II) Porphyrins as O_2-Coordination Sites

Rong-Min Wang,[†,‡] Teruyuki Komatsu,[†] Akito Nakagawa,[†] and Eishun Tsuchida*[,†]

Advanced Research Institute for Science and Engineering, Waseda University, 3-4-1 Okubo, Shinjuku-ku, Tokyo 169-8555, Japan, and Institute of Polymer, Northwest Normal University, Lanzhou 730070, China . Received June 17, 2004; Revised Manuscript Received September 25, 2004

Tetrakis{(α,α,α,α-*o*-pivalamido)phenyl}porphinatoiron(II) with a bifunctional tail possessing an axially coordinated imidazolyl group and a protein attachable succinimidyl(glutamyl) group (FeP-GluSu) has been synthesized. It can efficiently react with the lysine residues of recombinant human serum albumin (rHSA), giving a new albumin–heme conjugate [rHSA(FeP-Glu)]. MALDI-TOFMS showed a distinct molecular ion peak at *m/z* 70 643, which indicates that three FeP-Glu molecules were covalently linked to the rHSA scaffold. The binding number of FeP-Glu is approximately three (mol/mol) and independent of the mixing ratio. The CD spectrum and Native PAGE revealed that the albumin structure remained unaltered after the covalent bonding of the hemes. This rHSA(FeP-Glu) conjugate can bind and release O_2 reversibly under physiological conditions (pH 7.3, 37 °C) in the same manner as hemoglobin and myoglobin. The O_2-adduct complex had a remarkably long lifetime ($\tau_{1/2}$: 5 h). The O_2-binding affinity [$P_{1/2}^{O_2}$: 27 Torr] was identical to that of human red cells. Laser flash photolysis experiments gave the O_2- and CO-association rate constants and suggested that there are two different geometries of the imidazole binding to the central ion.

Human serum albumin (HSA), which is the major plasma protein component in our bloodstream, has no prosthetic group; however it nonspecifically captures many endogenous and exogenous compounds by weak interactions, *e.g.,* H-bond, ionic attraction, and hydrophobic interaction, namely noncovalent bonds (*1*–*3*). Synthetic heme, 2-[{8-*N*-(2-methylimidazolyl)octanoyl}-oxy]methyl-5,10,15,20-tetrakis{(α,α,α,α-*o*-pivalamido)-phenyl}porphinatoiron(II) (FeP, Chart 1 a) is also incorporated into recombinant HSA (rHSA), and the obtained albumin–heme (rHSA-FeP) hybrid can reversibly coordinate O_2 under physiological conditions (pH 7.3, 37 °C) (*4*). This O_2-carrying plasma hemoprotein could be of medical importance as a blood replacement composition (*4e*–*g*). Nevertheless, the major driving force of the heme-binding to albumin is a hydrophobic interaction; therefore, its binding constants (10^4–10^6 M^{-1}) are not high enough to maintain the heme concentration in the circulatory system for a long period (*4a*). The administration of the albumin–heme hybrid solution into rats demonstrated that the lifetimes of the heme was less than 6 h (*4e, 5*). To immobilize the heme group to the albumin scaffold more tightly and retain its O_2-transport efficacy, we have combined the O_2-coordination site FeP to the rHSA structure through a covalent bond. In this communication, we report, for the first time, the synthesis of a novel FeP analogue with a bifunctional branched-tail including an axially coordinated imidazolyl group and a protein-attachable succinimidyl(glutamyl) group (FeP-GluSu, Chart 1 a), and the properties of the rHSA conjugate bearing covalently linked FeP-Glu as a new O_2-carrying hemoprotein.

Chart 1. (a) 5,10,15,20-Tetrakis{(α,α,α,α-*o*-pivalamido)-phenyl}porphinatoiron Derivatives with a Bifunctional Tail Group. (b) Space-Filling Representation of the Oxygenated FeP-GluSu by Insight II (see ref 11)

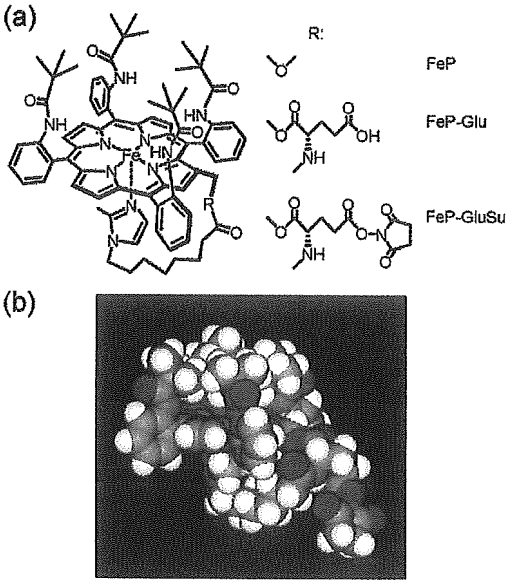

As a functional side-chain of FeP, which directly makes a covalent bond to rHSA, we selected the succinimidyl group, because it selectively reacts with the NH_2 group of lysine in the range of pH 6.3–8.6 with high yield. The branched tail that includes the imidazolyl and succnimidyl groups via a glutamate junction was introduced into the parent porphyrin **1** (*6*) as shown in Scheme 1 (*7*).

* Corresponding author. Phone: +81 3-5286-3120. Fax: +81-3-3205-4740. E-mail: eishun@waseda.jp.
† Waseda University.
‡ Northwest Normal University.

10.1021/bc049859m CCC: $30.25
Published on Web 11/12/2004

Scheme 1. Synthetic Scheme of FeP-GluSu

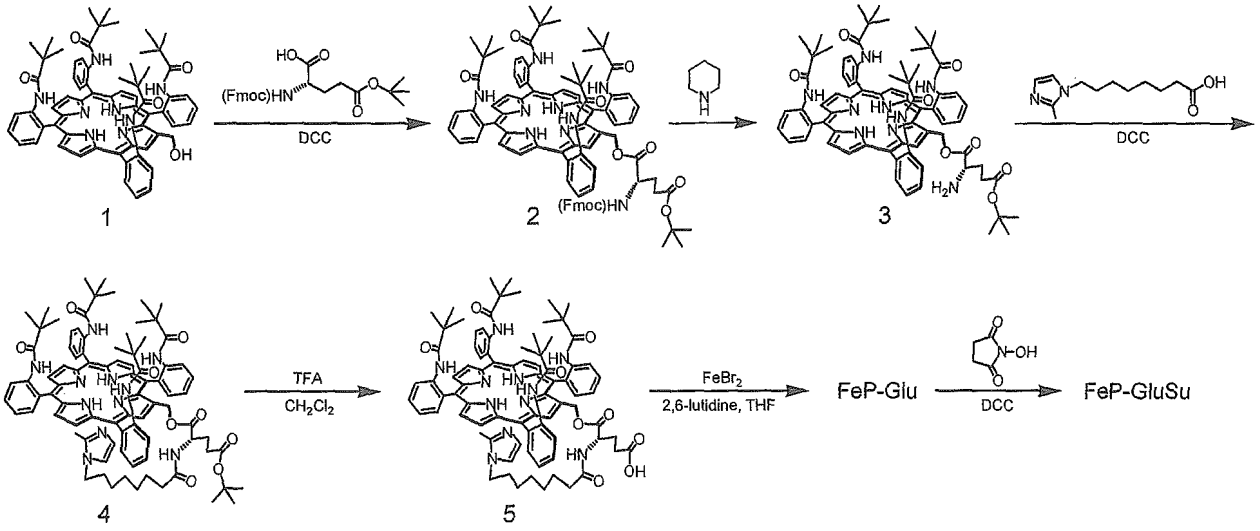

Table 1. CO-and O_2-Binding Parameters of rHSA(FeP-Glu) Conjugate in Phosphate–Buffered Solution (pH 7.3) at 25 °C

	$10^{-6}\,k_{on}^{CO}(M^{-1}s^{-1})$		$10^{-7}\,k_{on}^{O_2}(M^{-1}s^{-1})$		$10^{-2}\,k_{off}^{O_2}(s^{-1})$		$P_{1/2}^{O_2}$(Torr)[a]
system	fast	slow	fast	slow	fast	slow	
rHSA(FeP-Glu) conjugate	6.2	1.1	2.8	–	3.3	–	9 (27)
rHSA-FeP hybrid[b]	4.7	0.66	3.2	1.0	7.2	2.2	13 (35)
Hb(T-state)α[c]	0.22	–	0.29	–	1.8	–	40

[a] At 37 °C in parenthesis. [b] From ref 4c. [c] From refs 13–15.

First, Fmoc-L-Glu(g-*tert*-butyl ester) was bound to the OH group at the *β*-pyrrolic position of the porphyrin **1** by DCC. After removal of the Fmoc protecting group with piperidine, 8-*N*-(2-methylimidazolyl)octanoic acid was reacted with the obtained compound **3** in CH_2Cl_2, giving the imidazolyl-tailed porphyrin (**4**). The *tert*-butyl group was then removed by TFA, and the central iron insertion was carried out by the general $FeBr_2$ method to afford the iron-porphryin FeP-Glu. Finally, the reaction of *N*-hydroxysuccinimide with DCC gave the FeP-GluSu. All reactions can be performed at room temperature with high yields. The analytical data of all compounds described above were satisfactory obtained (*7*).

The FeP-Glu was converted to the ferrous complex by reduction in a heterogeneous two-phase system (toluene/aqueous $Na_2S_2O_4$) under an N_2 atmosphere (*6, 8*). The UV–vis absorption spectrum of the orange solution showed five-*N*-coordinated Fe(II) species (λ_{max}: 440, 531, 563 nm) via intramolecular imidazole binding (*6, 8, 9*). Upon exposure to CO, its UV–vis absorption immediately moved to that of the CO adduct complex. On the other hand, the dioxygenation was unstable at 25 °C, which is likely due to the presence of the neighboring glutamic acid proton.

The EtOH solution of the carbonyl FeP-GluSu (2 mL) was then injected into the phosphate-buffered solution of rHSA (8 mL, pH 7.3) (molar ratio 4/1), and the mixture was gently stirred for 1 h at room temperature. The solution was dialyzed against phosphate buffer (pH 7.3) to remove EtOH. The MALDI-TOFMS demonstrated a single molecular ion peak at *m/z* 70 643 (Figure 1). Attempts to measure the molecular weight of the rHSA-FeP hybrid, in which the FePs are noncovalently accommodated, failed using MALDI- and ESI-TOFMS; the molecular ion peak of rHSA (65 500) was only observable because the FePs are dissociated from the albumin during the ionization process (*10*). Therefore, we can conclude that the FeP-Glu is conjugated with rHSA

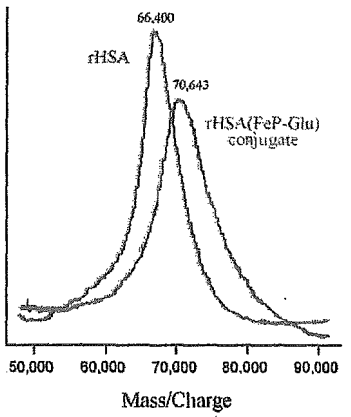

Figure 1. MALDI-TOFMS of the rHSA(FeP-Glu) conjugate. Matrix: 2,5-dihydroxybenzoic acid.

through amide bond formation. The average number of FeP-Glu in an rHSA was estimated to be 2.9–3.5, and this number is not dependent on the mixing molar ratio of FeP-GluSu/rHSA that ranged from 4 to 10. There are a total of 59 NH_2 groups in the rHSA structure, but only three of them are presumably active for the FeP-GluSu binding.

The conjugation of FeP-GluSu did not induce any change in the circular dichroism spectrum of rHSA in the 200–250 nm region. The Native PAGE of rHSA(FeP-Glu) also showed a single band with same migration distance of rHSA. Both results suggested that the secondary structure, molecular shape, and surface charge of albumin remained unaltered after the covalent binding of the hemes.

The UV–vis absorption spectrum of the rHSA(FeP-Glu) conjugate under an N_2 atmosphere showed a typical five-*N*-coordinated complex as seen in the toluene solution of FeP-Glu (Figure 2) (*4a,b, 6, 8, 9*). Upon exposure

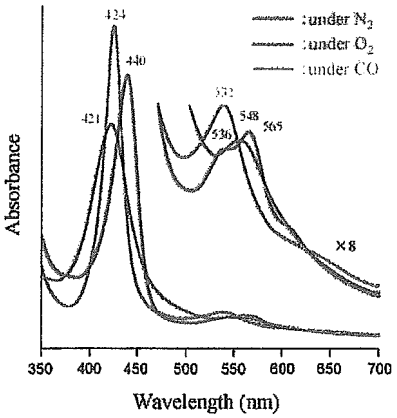

Figure 2. UV–vis absorption spectral changes of the rHSA-(FeP-Glu) conjugate in phosphate-buffered solution (pH 7.3) at 25 °C.

of this solution to O_2, the spectrum changed to that of the O_2-adduct complex under physiological conditions (pH 7.3, 37 °C) (*4a–c*). This dioxygenation was reversibly observed to be dependent on the O_2 partial pressure in the same manner as hemoglobin (Hb) and myoglobin. The half-lifetime of the O_2 adduct (ca. 5 h at 37 °C) was significantly longer than that of the noncovalent rHSA-FeP hybrid ($\tau_{1/2}$: 2 h) (*4d*). The covalent linkages of FeP-Glu to the protein scaffold obviously retarded the oxidation process of the central ferrous ion. Molecular simulation of the structure of FeP-GluSu revealed that the geometry of the imidazole ring against the porphyrin platform was perpendicular, which suggests that the spacer moiety between the imidazole and the porphyrin periphery does not produce an unfavorable distortion of the axial coordination and will not influence the O_2-binding behavior (see Chart 1b) (*11*).

The O_2-binding affinity [$P_{1/2}{}^{O_2}$] of the rHSA(FeP-Glu) conjugate was determined to be 27 Torr at 37 °C (*3b,c, 6, 7, 9, 10*), which is almost the same as that of the rHSA-FeP hybrid [$P_{1/2}{}^{O_2}$: 33 Torr] (*3b–d*) and identical to that of human red cells (*12*). The laser flash photolysis experiments provided the association rate constants of the O_2- and CO-bindings ($k_{on}{}^{O_2}$, $k_{on}{}^{CO}$) (*6, 8, 9a*). The absorption decays accompanying the O_2- and CO-recombination to the noncovalent rHSA-FeP hybrid were composed of two phases of the first-order kinetics, and the curves were fit by a double-exponential equation to determine k_{on} (fast) and k_{on} (slow) (Table 1) (*4c*). We supposed that the O_2- and CO-association to the FeP in the hydrophobic domains of the albumin was influenced by the molecular microenvironments around each O_2-coordination site, e.g., steric hindrance of the amino acid residue and difference in polarity (*4b–d*). The time dependence of the absorption change in the CO recombination to the rHSA(FeP-Glu) conjugate also showed double-exponential profile, but the rebinding process of O_2 obeyed monophasic decay. On the basis of studies on synthetic model hemes, it has been known that the proximal-side effect is the only primary factor which influences the association rate for CO but not for O_2 (*8, 9a*). We assume that there are two different geometries of the imidazole coordination and that each one shows the individual kinetics of the CO association. The covalent linkages between the axially coordinated imidazolyl side-chain and the albumin structure may provide an additional strain of the Fe–N(imidazole) bond and gives two conformations of the proximal-base binding. Since the $k_{on}{}^{O_2}$ value of rHSA(FeP-Glu) was nearly the same as the $k_{on}{}^{O_2}$ (fast) of the rHSA-FeP hybrid (Table 1), the FeP-Glu molecules are likely to locate on the surface of rHSA.

In conclusion, reaction of the newly synthesized tetrakis{(α,α,α,α-*o*-pivalamido)phenyl}porphinatoiron(II) with a proximal base and succinimidyl(glutamyl) group to rHSA produced a novel albumin conjugate bearing covalently attached heme groups as O_2-coordination sites. The molecular weight of rHSA(FeP-Glu) was directly measured by MALDI-TOF MS. In nature, one can find unique heme-linked proteins, e.g., cyctochrome *c*. The rHSA(FeP-Glu) conjugate presumably becomes a valuable model of these hemoproteins. The obtained rHSA-(FeP-Glu) can reversibly absorb O_2 under physiological conditions, and its O_2-binding affinity showed an identical value to that for human erythrocytes. These results suggest that this novel plasma protein may efficiently transport O_2 in the bloodstream as an O_2-carrier with a long circulation time.

ACKNOWLEDGMENT

This work was partially supported by Grant-in-Aid for Scientific Research (No. 16350093) from JSPS, Grant-in-Aid for Exploratory Research (No. 16655049) from MEXT Japan, and Health Science Research Grants (Regulatory Science) from MHLW Japan. R.M.W. acknowledges NNSFC (No. 20274034). The authors are grateful to NIPRO Corp. for their supporting the oxygen-infusion project.

Supporting Information Available: Experimental details of the compounds **2**, **3**, **4**, **5**, FeP-Glu, and FeP-GluSu and their spectroscopic data. This material is available free of charge via the Internet at http://pubs.acs.org.

LITERATURE CITED

(1) Peters, T., Jr. (1996) All about albumin. *Biochemistry, Genetics, and Medical Applications*, Academic Press, San Diego; and reference therein.

(2) Kragh-Hansen, U. (1981) Molecular aspects of ligand binding to serum albumin. *Pharmacol. Rev. 33,* 17–53.

(3) Curry, S., Brick, P., and Franks, N. P. (1999) Fatty acid binding to human serum albumin: new insights from crystallographic studies. *Biochim. Biphys. Acta 1441,* 131–140.

(4) (a) Komatsu, T., Hamamatsu, K., Wu, J., and Tsuchida, E. (1999) Physicochemical properties and O_2-coordination structure of human serum albumin incorporating tetrakis(*o*-pivamido)phenylporphyrinatoiron(II) Derivatives. *Bioconjugate Chem. 10,* 82–86. (b) Tsuchida, E., Komatsu, T., Matsukawa, Y., Hamamatsu, K., and Wu, J. (1999) Human serum albumin incorporating tetrakis(*o*-pivalamido)phenylporphinatoiron(II) derivative as a totally synthetic O_2-carrying hemoprotein. *Bioconjugate Chem. 10,* 797–802. (c) Komatsu, T., Matsukawa, Y., and Tsuchida, E. (2000) Kinetics of CO- and O_2-binding to human serum albumin-heme hybrid. *Bioconjugate Chem. 11,* 772–776. (d) Komatsu, T., Matsukawa, Y., and Tsuchida, E. (2002) Effect of heme structure on O_2-binding properties of human serum albumin-heme hybrids: intramolecular histidine coordination provides a stable O_2-adduct complex. *Bioconjugate Chem. 13,* 397–402. (e) Tsuchida, E., Komatsu, T., Hamamatsu, K., Matsukawa, Y., Tajima, A., Yoshizu, A., Izumi, Y., and Kobayashi, K. (2000) Exchange transfusion of albumin-heme as an artificial O_2-infusion into anesthetized rats: physiological responses, O_2-delivery and reduction of the oxidized hemin sites by red blood cells. *Bioconjugate Chem. 11,* 46–50. (f) Kobayashi, K., Komatsu, T., Iwamaru, A., Matsukawa, Y., Watanabe, M., Horinouchi, H., and Tsuchida, E. (2003) Oxygenation of hypoxia region in solid tumor by administration of human serum albumin incorporating synthetic hemes. *J. Biomed. Mater. Res. 64A,* 48–51. (g) Tsuchida, E., Komatsu, T., Matsukawa, Y., Nakagawa, A., Sakai, H., Kobayashi, K., and Suematsu, M. (2003) Human serum albumin incorporating synthetic heme: red blood cell substitute

without hypertension by nitric oxide scavenging. *J. Biomed. Mater. Res. 64A*, 257–261.
(5) Russo, S. M., Pepe, J. Y., Donohue, S., Cable E. E., Lambrecht, R. W., and Bonkovsky, H. L. (1995) Tissue distribution of zinc-mesoporphyrin in rats: relationship to inhibition of heme oxygenase. *J. Pharmacol. Exp. Ther. 272*, 766–774.
(6) Tsuchida, E., Komatsu, T., Ando, K., Kumamoto, S., and Nishide, H (1995) Synthesis and O_2-binding properties of tetraphenylporphyrinatoiron(II) derivatives bearing a proximal imidazole covalently bound at the β-pyrrolic position. *J. Chem. Soc., Perkin Trans. 2* 1995, 747–753.
(7) The synthetic details and spectroscopic data of the porphyrins can be obtained from the Supporting Information.
(8) Tsuchida, E., Komatsu, T., Arai, K., and Nishide, H. (1993) Synthesis and dioxygen-binding properties of double-sided porphyrinatoiron(II) complexes bearing covalently bound axial imidazole. *J. Chem. Soc., Dalton Trans.* 2465–2469.
(9) (a) Collman, J. P., Brauman, J. I., Collins, T. J., Iverson, B. L., Lang, G., Pettman, R. B., Sessler, J. L., and Walters, M. A. (1983) Synthesis and characterization of the "Pocket" porphyrins. *J. Am. Chem. Soc. 105*, 3038–3052. (b) Collman, J. P., Brauman, J. I., Iverson, B. L., Sessler, J. L., Morris, R. M., and Gibson, Q. H. (1983) O_2 and CO binding to iron(II) porphyrins: a comparison of the "Picket Fence" and "Pocket" porphyrins. *J. Am. Chem. Soc. 105*, 3052–3064.
(10) Tsuchida, E., Komatsu, T., and Yanagimoto, T. (2000) Molecular environment effect on O_2-binding to lipidporphyrinatoiron(II) complexes in aqueous media, *J. Porphyr. 4*, 81–87.
(11) The esff force field simulation was performed using an Insight II system (Molecular Simulations Inc.). The structure was generated by alternative minimizations and annealing dynamic calculations from 1,000 K to 100 K.
(12) Severinghaus, J. W. (1966) Blood gas calculator. *J. Appl. Physiol. 21*, 1108–1116.
(13) Sawicki, C. A., and Gibson G. H. (1977) Properties of the T State of Human Oxyhemoglobin Studied by Laser Photolysis. *J. Biol. Chem. 252*, 7538–7547.
(14) Sharma, V. S., Schmidt, M. R., and Ranney, H. M. (1976) Dissociation of CO from Carboxyhemoglobin. *J. Biol. Chem. 251*, 4267–4272.
(15) Steinmeier, R. C., and Parkhurst, L. J. (1975) Kinetic Studies on the Five Principle Components of Normal Adult Human Hemoglobin. *Biochemistry 14*, 1564–1573.

BC049859M

J|A|C|S
ARTICLES
Published on Web 10/20/2005

O_2 and CO Binding Properties of Artificial Hemoproteins Formed by Complexing Iron Protoporphyrin IX with Human Serum Albumin Mutants

Teruyuki Komatsu,*,† Naomi Ohmichi,† Akito Nakagawa,† Patricia A. Zunszain,‡ Stephen Curry,‡ and Eishun Tsuchida*,†

Contribution from the Advanced Research Institute for Science and Engineering, Waseda University, 3-4-1 Okubo, Shinjuku-ku, Tokyo 169-8555, Japan, and Division of Cell and Molecular Biology, Faculty of Life Sciences, Imperial College London, Huxley Building, South Kensington Campus, London SW7 2AZ, United Kingdom

Received July 18, 2005; E-mail: teruyuki@waseda.jp; eishun@waseda.jp

Abstract: The binding properties of O_2 and CO to recombinant human serum albumin (rHSA) mutants with a prosthetic heme group have been physicochemically and kinetically characterized. Iron(III) protoporphyrin IX (hemin) is bound in subdomain IB of wild-type rHSA [rHSA(wt)] with weak axial coordination by Tyr-161. The reduced ferrous rHSA(wt)−heme under an Ar atmosphere exists in an unusual mixture of four- and five-coordinate complexes and is immediately autoxidized by O_2. To confer O_2 binding capability on this naturally occurring hemoprotein, a proximal histidine was introduced into position Ile-142 or Leu-185 by site-directed mutagenesis. A single mutant (I142H) and three double mutants (I142H/Y161L, I142H/Y161F, and Y161L/L185H) were prepared. Both rHSA(I142H/Y161L)−heme and rHSA(I142H/Y161F)−heme formed ferrous five-*N*-coordinate high-spin complexes with axial ligation of His-142 under an Ar atmosphere. These artificial hemoproteins bind O_2 at room temperature. Mutation at the other side of the porphyrin, Y161L/L185H, also allowed O_2 binding to the heme. In contrast, the single mutant rHSA(I142H)−heme could not bind O_2, suggesting that removal of Y161 is necessary to confer reversible O_2 binding. Laser flash photolysis experiments showed that the kinetics of CO recombination with the rHSA(mutant)−heme were biphasic, whereas O_2 rebinding exhibited monophasic kinetics. This could be due to the two different geometries of the axial imidazole coordination arising from the two orientations of the porphyrin plane in the heme pocket. The O_2 binding affinities of the rHSA(mutant)−heme were significantly lower than those of hemoglobin and myoglobin, principally due to the high O_2 dissociation rates. Changing Leu-161 to Phe-161 at the distal side increased the association rates of both O_2 and CO, which resulted in enhanced binding affinity.

Introduction

Human serum albumin (HSA) is a versatile protein found at high concentrations (4−5 g/dL) in blood plasma and is principally characterized by its remarkable ability to bind a wide range of insoluble endogenous and exogenous compounds.[1] Physiological ligands for HSA include nonesterified fatty acids, hemin, bilirubin, bile acids, and thyroxine,[2−4] but the protein also binds a huge variety of drugs. Currently, it is of great interest to exploit the carrier properties of this shuttle protein for the development of novel therapeutic reagents for drug delivery and pharmacodynamic modulation.[5−7] Hemin [iron(III) protoporphyrin IX] released from hemoglobin (Hb) during the enucleation of red cells or through hemolysis is captured by HSA, which has a high binding constant for this ligand ($K \approx 10^8$ M^{-1}).[8] This strong affinity of HSA for hemin has stimulated efforts to develop albumin as an artificial hemoprotein which can mimic the O_2 binding capability of Hb and myoglobin (Mb).[9,10] HSA consists of a helical monomer of 66.5 kDa containing three homologous domains (I−III), each of which

† Waseda University.
‡ Imperial College London.

(1) Peters, T. *All about Albumin: Biochemistry, Genetics and Medical Applications*; Academic Press: San Diego, 1996; and references therein.
(2) (a) Kragh-Hansen, U. *Pharmacol. Rev.* **1981**, *33*, 17−53. (b) Kragh-Hansen, U. *Danish Med. Bull.* **1990**, *37*, 57−84.
(3) (a) Curry, S.; Madelkow, H.; Brick, P.; Franks, N. *Nat. Struct. Biol.* **1998**, *5*, 827−835. (b) Bhattacharya, A. A.; Grune, T.; Curry, S. *J. Mol. Biol.* **2000**, *303*, 721−732. (c) Curry, S. Plasma Albumin as a Fatty Acid Carrier. In *Adv. Mol. Cell. Biol.*; van der Vusse, G., Ed.; Elsevier: 2003; Vol. 33, pp 29−46. (d) Petitpas, I.; Petersen, C. E.; Ha, C.-E.; Bhattacharya, A. A.; Zunszain, P. A.; Ghuman, J.; Bhagavan, N. V.; Curry, S. *Proc. Natl. Acad. Sci. U.S.A.* **2003**, *100*, 6440−6445. (e) Zunszain, P. A.; Ghuman, J.; Komatsu, T.; Tsuchida, E.; Curry, S. *BMC Struct. Biol.* **2003**, *3*, 6.
(4) (a) He, X. M.; Carter, D. C. *Nature* **1992**, *358*, 209−215. (b) Carter, D. C.; Ho, J. X. *Adv. Protein Chem.* **1994**, *45*, 153−203. (c) Wardell, M.; Wang, Z.; Ho, J. X.; Robert, J.; Ruker, F.; Rubel, J.; Carter, D. C. *Biochem. Biophys. Res. Commun.* **2002**, *291*, 813−819.
(5) Beljaars, L.; Molema, G.; Schuppan, D.; Geerts, A.; De Bleser, P. J.; Weert, B.; Meijer, D. K. F.; Poelstra, K. *J. Biol. Chem.* **2000**, *275*, 12743−12751.
(6) Kurtzhals, P.; Havelund, S.; Jonassen, I.; Kiehr, B.; Larsen, U. D.; Ribel, U.; Markussen, J. *Biochem. J.* **1995**, *312*, 725−731.
(7) Sheffield, W. P. *Curr. Drug Targets Cardiovasc. Haematol. Disord.* **2001**, *1*, 1−22.
(8) Adams, P. A.; Berman, M. C. *Biochem. J.* **1980**, *191*, 95−102.
(9) (a) Komatsu, T.; Hamamatsu, K.; Wu, J.; Tsuchida, E. *Bioconjugate Chem.* **1999**, *10*, 82−86. (b) Tsuchida, E.; Komatsu, T.; Matsukawa, Y.; Hamamatsu, K.; Wu, J. *Bioconjugate Chem.* **1999**, *10*, 797−802. (c) Komatsu, T.; Matsukawa, Y.; Tsuchida, E. *Bioconjugate Chem.* **2002**, *13*, 397−402.

10.1021/ja054819u CCC: $30.25

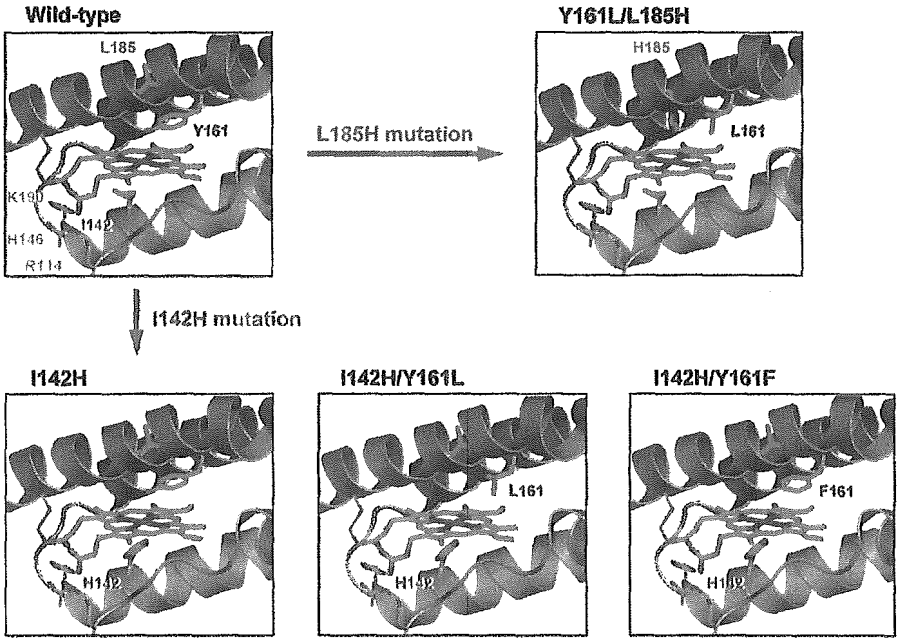

Figure 1. Structural models of the effect of site-directed mutagenesis in subdomain IB of HSA to construct a tailor-made heme pocket, which allows O_2 binding to the prosthetic Fe^{2+} protoporphyrin IX (heme) group.[12]

is composed of A and B subdomains. Crystallographic studies have revealed that hemin is bound within a narrow D-shaped hydrophobic cavity in subdomain IB with axial coordination of Tyr-161 to the central ferric ion and electrostatic interactions between the porphyrin propionates and a triad of basic amino acid residues (Arg-114, His-146, and Lys-190) (Figure 1).[3e,4c] In terms of the general hydrophobicity of this α-helical heme pocket, the subdomain IB of HSA potentially has similar features to the heme binding site of Hb or Mb. However, if one reduces the HSA−hemin to obtain the ferrous complex, it is rapidly oxidized by O_2 even at low temperature (~0 °C). This is due to the fact that HSA lacks the proximal histidine which in Hb and Mb enables the prosthetic heme group to bind O_2 and serves to regulate the O_2 binding affinity.

On the basis of the crystal structure of the HSA−hemin complex, we have used site-directed mutagenesis to introduce into the heme binding site of HSA a histidine that would be predicted to provide axial coordination to the central Fe^{2+} atom of the heme and thereby promote O_2 binding (Figure 1). An initial recombinant HSA mutant, in which Ile-142 and Tyr-161 were replaced by His and Leu, respectively [rHSA(I142H/Y161L)], has been made, and the O_2 binding capabilities of the heme complex have been partially evaluated.[11] In the present study, we have elucidated the coordination structure of the naturally occurring wild-type rHSA−heme [rHSA(wt)−heme] by UV−vis and magnetic circular dichroism (MCD) spectroscopies and characterized the unusual axial coordination of Tyr-161 to the heme. To develop HSA−heme as a synthetic O_2 carrier, we have also generated several new mutant rHSA−heme complexes. Their O_2 and CO binding properties have been characterized kinetically and compared to those of the natural Hb, Mb, and recombinant Mb (rMb) mutants. We have shown that our mutagenesis approach can create a new class of albumin-based artificial hemoproteins which would serve as an O_2 carrier.

Experimental Section

Materials and Apparatus. rHSA(wt) was kindly provided by the NIPRO Corp. (Osaka, Japan). All reagents were purchased from commercial sources as special grades and used without further purification unless otherwise noted. Iron(III) protoporphyrin IX (hemin) chloride was purchased from Fluka. Horse skeletal muscle myoglobin (Mb) was purchased from Sigma-Aldrich. The iron(III) protoporphyrin IX dimethyl ester chloride (FePPIXDME) was prepared by esterification of carboxylate side chains of hemin with acidic methanol. The UV−vis absorption spectra were recorded using an Agilent 8453 UV−visible spectrophotometer fitted with an Agilent 89090A temperature control unit.

Site-Directed Mutagenesis, Protein Expression, and Purification. Specific mutations were introduced into HSA within the context of a plasmid vector containing the entire HSA coding region (pHIL-D2 HSA) using designed primers with the QuikChange XL site-directed mutagenesis kit (Stratagene).[13] All mutations were confirmed by DNA sequencing. Each mutated pHIL-D2 HSA plasmid was linearized by NotI digestion and introduced into *Pichia pastoris GS115* by electroporation using a BioRad MicroPulser. Expressions were carried out by standard protocols (Invitrogen) with some modifications. Clones were grown upon BMGY medium [1% yeast extract, 2% peptone, 0.1 M potassium phosphate (pH 6.0), 1.34% yeast nitrogen base without amino acids, 40 ppm biotin, 1% glycerol] and transferred to BMMY medium [1% yeast extract, 2% peptone, 0.1 M potassium phosphate (pH 6.0), 1.34% yeast nitrogen base without amino acids, 40 ppm biotin, 1% methanol] for induction with methanol in baffled shaking flasks at 30 °C in a JEIOTECH SI-600R incubator at 200 rpm.

(10) Marden, M. C.; Hazard, E. S.; Leclerc, L.; Gibson, Q. H. *Biochemistry* **1989**, *28*, 4422−4426.
(11) Komatsu, T.; Ohmichi, N.; Zunszain, P. A.; Curry, S.; Tsuchida, E. *J. Am. Chem. Soc.* **2004**, *126*, 14304−14305.
(12) The pictures were produced on the basis of crystal structure coordinate of the rHSA(wt)-hemin (code: 1O9X, ref 3e) using PyMOL. DeLano, W. L. The PyMOL Molecular Graphics System 2002 DeLano Scientific, San Carlos, CA.
(13) (a) Peterson, C. E.; Ha, C.-E.; Jameson, D. M.; Bhagavan, N. V. *J. Biol. Chem.* **1996**, *271*, 19110−19117. (b) Peterson, C. E.; Ha, C.-E.; Harohalli, K.; Park, D.; Bhagavan, N. V. *Biochemistry* **1997**, *36*, 7012−7017.

The secreted rHSA was isolated as follows. The growth medium was centrifuged to harvest the culture supernatant, which was brought to 50% saturation by the addition of solid ammonium sulfate with stirring at room temperature. The mixture was then incubated at 4 °C for 1 h. The resulting precipitate was removed by centrifugation, and the supernatant fluid was brought to 95% saturation with ammonium sulfate. The precipitated protein, which contains rHSA, was collected by centrifugation and dissolved in distilled water. The brownish solution was dialyzed for 48 h at 4 °C against 100 volumes of distilled water, followed by 24 h against 100 volumes of 50 mM potassium phosphated buffer (pH 7.0). The dialysate was then loaded onto a Cibacron Blue column of Blue Sepharose 6 Fast Flow (Amersham Pharmacia Biotech) and washed with 10 bed volumes of 50 mM potassium phosphate. Elution of the rHSA(mutant) was carried out with 3 M NaCl and the eluent dialyzed against 50 mM potassium phosphate. After concentration using an ADVANTEC Q0100 ultrafilter (10 kDa Mw cutoff) in an UHP-43K ultraholder, the samples were applied to a Superdex 75 column (Amersham Pharmacia Biotech) using 50 mM potassium phosphate as the running buffer. All the purification steps were followed by SDS–PAGE analysis. Each rHSA(mutant) exhibited a single band and migrated the same distance as rHSA(wt). The protein concentration was assayed by measuring the absorbance at 280 nm ($\epsilon_{280} = 3.4 \times 10^4$ M^{-1} cm^{-1}).

Preparations of rHSA–Hemin and rHSA–Heme Complexes. The ferric rHSA(mutant)–hemin complexes were prepared according to our previously reported procedures for rHSA(wt)–hemin.[3e] Typically 5 mL of 0.1 mM rHSA(mutant) in 50 mM potassium phosphate (pH 7.0) was mixed with 0.8 mL of 0.688 mM hemin in DMSO [hemin:rHSA(mutant) molar ratio of 1.1] and incubated overnight with rotation in the dark at room temperature. The complex was then diluted with 50 mM potassium phosphate (200 mL) and concentrated to the initial volume (5.8 mL) using an ADVANTEC Q0100 ultrafilter (10 kDa Mw cutoff). These dilution and concentration cycles were repeated to reduce the final concentration of DMSO to <0.1 vol %. The resulting samples were analyzed by a SDS–PAGE to confirm the protein integrity and concentration.

The 50 mM phosphate-buffered solution (pH 7.0) of rHSA(mutant)–hemin ([hemin] = ca. 10 μM) in a 10 mm path length optical quartz cuvette sealed with a rubber septum was purged with Ar for 40 min. A small excess amount of degassed aqueous sodium dithionate was added by microsyringe to the sample under an Ar atmosphere to reduce the central ferric ion of the hemin, generating the deoxy ferrous rHSA(mutant)–heme complexes.

Kinetic Measurements for O_2 and CO Bindings. Kinetics studies were carried out using laser flash photolysis techniques at 22 °C, except for the determination of the CO dissociation rates. Laser flash photolysis experiments were performed using a Unisoku TSP-1000WK time-resolved spectrophotometer with a Spectron Laser Systems SL803G-10 Q-switched Nd:YAG laser, which generated a second-harmonic (532 nm) pulse of 6 ns duration (10 Hz). The probe light from a 150 W xenon arc-lamp was passed through an UV cutoff filter and an Asahi Spectra MC filter before irradiation to minimize any sample damage. Normally, fresh solutions of the deoxy rHSA(mutant)–heme were made up for each set of experiments, and the gas mixture with the desired partial pressure of O_2/CO/N_2 prepared by a KOFLOC Gasblender GB-3C was flowed into the sample cuvette for 20 min for equilibration.

In general, recombination following laser flash photolysis to $heme O_2$ or hemeCO occurs according to eq 1 with the association rate constant (k_{on}^{L}), dissociation rate constant (k_{off}^{L}), and apparent rate constant (k_{app}) given by eq 2.[14,15] The values of k_{app} were obtained directly from the log plots of the change in absorbance (ΔA) versus time. The gas

$$\text{hemeL} \xrightarrow{h\nu} \text{heme} \underset{k_{off}^{L}}{\overset{k_{on}^{L}}{\rightleftharpoons}} \text{hemeL} \quad [\text{L} = \text{O}_2 \text{ or CO}] \tag{1}$$

$$k_{app} = k_{on}^{L}[\text{L}] + k_{off}^{L} \tag{2}$$

concentrations were always higher than that of the heme; therefore, the pseudo-first-order approximation can be applied throughout. For CO rebinding at high [CO], eq 2 reduces to eq 3 because $k_{on}^{CO}[CO] \gg k_{off}^{CO}$.

$$k_{app} \approx k_{on}^{CO}[CO] \tag{3}$$

Thus, k_{on}^{CO} of the rHSA(mutant)–heme was easily calculated from k_{app}/[CO].

The O_2 association rates ($k_{on}^{O_2}$) and the O_2 binding constants [$K^{O_2} = (P_{1/2}^{O_2})^{-1}$] of the rHSA(mutant)–heme were measured using the competitive rebinding technique.[14,15] Photolysis of hemeCO in the presence of CO and O_2 gives the five-*N*-coordinate heme (deoxy state), which is first trapped as $heme O_2$ and subsequently converted back to hemeCO (eq 4).

$$\text{hemeCO} \underset{k_{on}^{CO}}{\overset{k_{off}^{CO}}{\rightleftharpoons}} \text{heme} \underset{k_{off}^{O_2}}{\overset{k_{on}^{O_2}}{\rightleftharpoons}} \text{heme}O_2 \tag{4}$$

The CO concentration was held constant, and the fast and slow kinetics were measured at different [O_2]. The fast process is given by eq 5, allowing the direct determination of $k_{on}^{O_2}$ from a plot of k_{app}(fast) versus [O_2].

$$k_{app}(\text{fast}) = k_{on}^{O_2}[O_2] + k_{off}^{O_2} + k_{on}^{CO}[CO] \tag{5}$$

The rate constant for the slower process, k_{app}(slow), is substituted into Traylor's eq 6 to obtain K^{O_2} [$=(P_{1/2}^{O_2})^{-1}$].[15]

$$\frac{k_{on}^{CO}[CO]}{k_{app}(\text{slow})} = K^{O_2}[O_2] + \frac{k_{on}^{CO}[CO]}{k_{off}^{O_2}} + 1 \tag{6}$$

The value of $k_{on}^{CO}[CO]$ is constant; therefore, the plots of $k_{on}^{CO}[CO]/k_{app}$(slow) versus [O_2] affords K^{O_2}.

The relaxation curves that accompanied the O_2 or CO recombination were fitted to single- or double-exponentials using the Unisoku Spectroscopy & Kinetics Software. The $k_{off}^{O_2}$ values can be determined from the *y*-intercept of eq 5 or 6, but they often have large deviations. Therefore, we calculated $k_{off}^{O_2}$ from $k_{on}^{O_2}/K^{O_2}$ (both obtained from slopes).

The CO dissociation from the rHSA(mutant)–hemeCO was measured by carrying out the replacement reaction with NO.[16] A Sephadex G-25 column was equilibrated with CO-saturated potassium phosphate buffer (50 mM, pH 7.0), and the rHSA(mutant)–hemeCO solution was passed through the column to remove the dithionate. The eluent was directly connected to a optical quartz cuvette under a 10% CO (in N_2) atmosphere. The 10% NO (in N_2) equilibrated buffer was then rapidly injected into the rHSA(mutant)–hemeCO solution, and the time dependence of the decrease in absorption at 418 nm was monitored. The relaxation curves that accompanied the CO dissociation within several minutes were analyzed by fitting to double-exponentials. The CO binding constants [$K^{CO} = (P_{1/2}^{CO})^{-1}$] were calculated using k_{on}^{CO}/k_{off}^{CO}.

Magnetic Circular Dichroism (MCD). The MCD for the 50 mM potassium phosphate-buffered solutions (pH 7.0) of the rHSA(wt)–heme and rHSA(mutant)–heme series (8.0 μM) under Ar and CO atmospheres were measured using a JASCO J-820 circular dichrometer fitted with a 1.5 T electromagnet at 22 °C. The spectrum was acquired five times to improve signal-to-noise, and each data point was corrected

(14) Collman, J. P.; Brauman, J. I.; Iverson, B. L.; Sessler, J. L.; Moris, R. M.; Gibson, Q. H. *J. Am. Chem. Soc.* **1983**, *105*, 3052–3064.
(15) Traylor, T. G.; Tsuchiya, S.; Campbell, D.; Mitchel, M.; Stynes, D.; Koga, N. *J. Am. Chem. Soc.* **1985**, *107*, 604–614.
(16) Rohlfs, R.; Mathews, A. J.; Carver, T. E.; Olson, J. S.; Springer, B. A.; Egeberg, K. D.; Sliger, S. G. *J. Biol. Chem.* **1990**, *265*, 3168–3176.

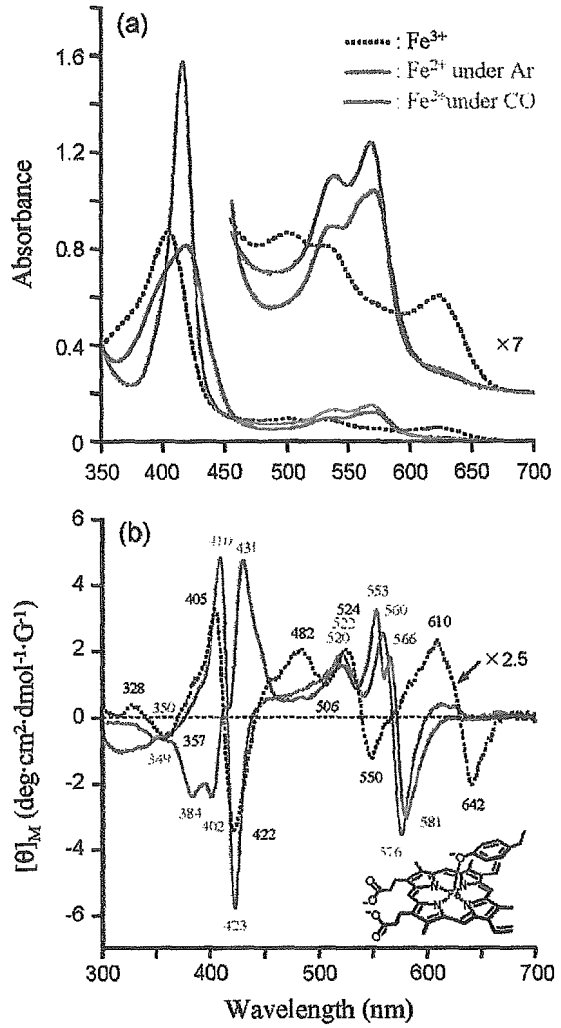

Figure 2. (a) UV−vis absorption and (b) MCD spectral changes of the rHSA(wt)-heme in 50 mM potassium phosphate buffered solution (pH 7.0, 22 °C).

by subtracting the optical rotation observed in the absence of an applied magnetic field.

Results and Discussion

Naturally Occurring rHSA(wt)−Hemin. Our crystal structure analysis revealed that hemin is bound within a D-shaped cavity in subdomain IB of rHSA(wt), where the central ferric ion is coordinated by Tyr-161, and the two propionate side chains are coordinated by a triad of basic amino acid residues (Figure 1).[3e] The UV−vis absorption spectrum of the phosphate-buffered solution (50 mM, pH 7.0) of rHSA(wt)−hemin showed a Soret band at 405 nm and the charge-transfer (CT) band of the porphyrin $p\pi$ to the Fe^{3+} $d\pi$ orbitals at 624 nm (Figure 2a). The spectral pattern and amplitudes were almost constant in the temperature range of 5−40 °C. The dominant feature of the spectrum was quite similar to those of the human or horse heart ferric H93Y recombinant Mb [rMb(H93Y)], in which the proximal histidine (His-93) was replaced with Tyr by site-directed mutagenesis (Table 1).[17,18] Adachi and co-workers showed that the ferric rMb(H93Y) formed a five-coordinate high-spin complex with a single oxygen donor of the proximal

Table 1. UV-vis Absorption Spectral Data of the rHSA(wt)-Heme, rHSA(mutant)-Heme and Other Hemoproteins

Hemoproteins	State	λ_{max} (nm) Soret	Visible
rHSA(wt)-Heme[a]	Fe^{3+}	405	501, 534, 624
	Fe^{2+}	419	538, 559(sh), 570
	$Fe^{2+}CO$	416	539, 568
HSA-Heme[b]	Fe^{3+}	404	498, 530, 620
	Fe^{2+}	416	534, 570
	$Fe^{2+}CO$	418	536, 568
Human rMb(H93Y)[c]	Fe^{3+}	402	480, 520(sh), 598
	Fe^{2+}	427	560
	$Fe^{2+}CO$	420	539, 567
Horse Heart rMb(H93Y)[d]	Fe^{3+}	403	487, 524, 599
	Fe^{2+}	429	556
	$Fe^{2+}CO$	419	539, 570
FePPIXDME(CH_3O^-)[e]	Fe^{3+}	401	476, 580(sh), 600
FePPIXDME(p-NO_2PhO^-)[f]	Fe^{3+}	402	500, 528, 621
FePPIXDME[a,g]	Fe^{3+}	400	571, 599
	Fe^{2+}	393, 414, 427, 440(sh)	535, 571
	$Fe^{2+}CO$	411	532, 564
rHSA(I142H)-Heme[a]	Fe^{3+}	404	501, 533, 619
	Fe^{2+}	424	530, 558
	$Fe^{2+}CO$	419	537, 560
rHSA(I142H/Y161L)-Heme[a]	Fe^{3+}	402	533, 620
	Fe^{2+}	426	531(sh), 559
	$Fe^{2+}O_2$	412	537, 573
	$Fe^{2+}CO$	419	538, 565
rHSA(I142H/Y161Y)-Heme[a]	Fe^{3+}	402	533, 620
	Fe^{2+}	425	532(sh), 559
	$Fe^{2+}O_2$	411	538, 576
	$Fe^{2+}CO$	419	538, 565
rHSA(Y161L/L185H)-Heme[a]	Fe^{3+}	408	528, 620
	Fe^{2+}	422	530, 558
	$Fe^{2+}O_2$	412	538, 570
	$Fe^{2+}CO$	419	537, 560
Mb[a,h]	Fe^{3+}	409	503, 548(sh), 632
	Fe^{2+}	434	557
	$Fe^{2+}O_2$	418	544, 581
	$Fe^{2+}CO$	423	541, 579

[a] In 50 mM potassium phosphate buffer (pH 7.0, 22 °C). [b] In 0.1 M phosphate buffer (pH 7.0); ref 22. [c] In 50 mM sodium phosphate buffer (pH 7.0, 20 °C); ref 17. [d] At pH 7−10, 25 °C; ref 18. [e] In CH_2Cl_2/CH_3OH = 9/1 (v/v) (25 °C); ref 21. [f] In CH_2Cl_2 (25 °C); ref 21. [g] In 0.5% Me_3CeNBr. [h] Horse muscle Mb (Sigma).

Tyr-93 by resonance Raman spectroscopy.[17b] Our absorption spectral data imply that the hemin is bound to Tyr-161 of rHSA-(wt) and forms a ferric five-coordinate high-spin complex under physiological conditions. Interestingly, the CT absorptions of the rHSA(wt)−hemin appeared at a higher wavelength (λ_{max} = 624 nm) compared to rMb(H93Y) (λ_{max} = 598−599 nm). Dawson and co-workers classified the CT bands of the oxygen-ligated hemins into two groups: the first at around 600 nm for rMb(H93Y) and the methoxide (CH_3O^-) complex of Fe^{3+} protoporphyrin IX dimethyl ester (Fe^{3+}PPIXDME), and the second at around 620 nm for p-nitrophenolate (p-NO_2PhO^-) or the acetate complex of Fe^{3+}PPIXDME, in which the nonoccupied π^* orbitals of the fifth ligand interacts with the Fe^{3+} $d\pi$ orbitals and, in turn, lowered the energy level of the CT transition (Table 1).[19] The rHSA(wt)−hemin definitely belongs to the latter group, which suggests that the axial coordination

(17) (a) Adachi, S.; Nagano, S.; Watanabe, Y.; Ishimori, K.; Morishima, I. *Biochim. Biophys. Res. Commun.* **1991**, *180*, 138−144. (b) Adachi, S.; Nagano, S.; Ishimori, K.; Watanabe, Y.; Morishima, I.; Egawa, T.; Kitagawa, T.; Makino, R. *Biochemistry* **1993**, *32*, 241−252.
(18) Hildebrand, D. P.; Burk, D. L.; Maurus, R.; Ferrer, J. C.; Brayer G. D.; Mauk, A. G. *Biochemistry* **1995**, *34*, 1997−2005.
(19) Pond, A. E.; Roach, M. P.; Sono, M.; Rux, A. H.; Franzen, S.; Hu, R.; Thomas, M. R.; Wilks, A.; Dou, Y.; Ikeda-Saito, M.; Oritz de Montellano, P. R.; Woodruff, W. H.; Boxer, S. G.; Dawson, J. H. *Biochemistry* **1999**, *38*, 7601−7608.

of Tyr-161 to the hemin is weaker than that of rMb(H93Y) and Fe^{3+}PPIXDME(CH_3O^-). This is consistent with the observation that the Fe^{3+}–O(phenolate) distance in the crystal structure of the rHSA(wt)–hemin (2.78 Å) is greater than that for rMb(H93Y) (1.91 Å).[3e]

We then employed MCD spectroscopy to elucidate the axial coordination environment of the rHSA(wt)–hemin. MCD is a powerful probe of the oxidation state, spin state, and the nature of the axial ligand in heme system and has frequently been used as a method of comparison between synthetic iron porphyrins of known axial ligation and newly discovered hemoproteins of unknown ligation.[20] The ferric rHSA(wt)–hemin showed a characteristic MCD pattern with two distinct troughs in the visible region (550, 642 nm) (Figure 2b), which was more similar to that of the five-coordinate Fe^{3+}PPIXDME (*p*-NO_2-PhO^-) than to that of the Fe^{3+}PPIXDME(CH_3O^-).[19,21] The MCD of the rHSA(wt)–hemin therefore also supports the formation of a five-coordinate high-spin hemin complex with weak axial ligation by Tyr-161.

Reduced Ferrous rHSA(wt)–Heme. Reduction of the ferric rHSA(wt)–hemin by the addition of sodium dithionate under an Ar atmosphere gave a ferrous heme complex with a broad Soret band at 419 nm ($\Delta\lambda_{1/2}$ = 61 nm) and two definite Q-bands at 538 and 570 nm (Figure 2a). This is in significant contrast to human ferrous rMb(H93Y) in a five-coordinate high-spin complex, which exhibits a similar spectrum to deoxy Mb with a sharp Soret band and single Q-band absorption around 560 nm (Table 1).[17,18] The shoulder at 559 nm in the spectrum of the rHSA(wt)–heme is probably due to a ferrous five-coordinate complex, but this clearly coexists with another species. One possible candidate is a six-coordinate low-spin complex. Casella and co-workers proposed that the reduced HSA–heme contains a six-coordinate heme.[22] Nevertheless, the MCD spectrum of the ferrous rHSA(wt)–heme (Figure 2b) was quite different from the well-known shape of the six-coordinate low-spin heme derivatives, such as cytochrome b_5 and bisimidazole-ligated Fe^{2+} PPIXDME, which show a sharp and intense Faraday *A* term corresponding to the α band.[20c]

Another possibility is a four-coordinate intermediate spin state (S = 1) not found in natural Mb. Phosphate-buffered solutions (pH 7.0) of 0.5% (w/v) *N*-cetyltrimethylammonium bromide ($CetMe_3NBr$) micelles containing dissolved Fe^{2+}PPIXDME showed a multiple broad Soret band ($\Delta\lambda_{1/2}$ = 73 nm) and well-defined β and α bands (535 and 571 nm) (Table 1, see Figure S1a), a spectral pattern consistent with a four-coordinate Fe^{2+}-mesoporphyrin IX dimethyl ester in the $CetMe_3NBr$ suspension.[23] This observation suggests that the strong β and α bands (538, 570 nm) in the UV–vis absorption spectrum of the rHSA(wt)–heme complex also derived from a ferrous four-coordinate complex. The micellar solution of Fe^{2+}PPIXDME showed complicated MCD bands in the Soret region and two positive peaks (522, 562 nm) and one trough (579 nm) in the visible region (see Figure S1b). The typical MCD of five-coordinate deoxy Mb is shown in Figure 4b (vide infra). Comparison of these data with the MCD spectral pattern of ferrous rHSA(wt)–heme suggests that the latter involves both important features of four- and five-coordinate heme complexes (Figure 2b). Therefore, we conclude that the reduced ferrous rHSA(wt)–heme is in an unusual mixture of a five-coordinate high-spin complex (S = $^5/_2$) with Tyr-161 and a four-coordinate intermediate spin state (S = 1) under an Ar atmosphere. The estimated ratio of the five- and four-coordinate complexes is approximately 1/1.

Upon the addition of O_2 gas to this solution, the central ferrous ion was rapidly autoxidized even at low temperature (~0 °C), and the UV–vis absorption spectrum returned to the initial ferric complex. On the other hand, a carbonyl complex was formed at room temperature and exhibited a very similar absorption (λ_{max} = 416, 539, 568 nm) to human and horse rMb(H93Y)CO (Figure 2a, Table 1).[17,18] The MCD spectrum of the rHSA(wt)–hemeCO showed simple Faraday *A* terms associated with the porphyrin π–π^* transitions, which are typical of a low-spin carbonyl heme (Figure 2b).[20] The rHSA(wt)–hemeCO could be a diamagnetic low-spin complex with a phenolate ligand (Tyr-161) similar to what was found for rMb(H93Y).

In our blood stream, the most avid carrier of hemin is the specific heme-binding protein, hemopexin.[24,25] The binding constant of hemopexin for hemin is 10^4-fold higher than HSA. However, due to the extremely low abundance of hemopexin in plasma (<17 μM), HSA acts as a significant depot of hemin in the circulation. The hemin binding to these proteins not only conserves the porphyrin iron and channels it to the specific catabolism site but it also prevents its toxic effects, such as the catalysis of hydroxyl radical production. Furthermore, HSA–hemin exhibits little peroxidase or catalase activities.[22] The weak axial coordination of phenolate to HSA-bound hemin may therefore have evolved for (1) easy release and transfer to hemopexin in the blood stream, and (2) maintenance of the antioxidative homeostasis in the extracellular fluids of our body.

Genetic Engineered rHSA(mutant) Complexed with Hemin. The detailed architecture of the heme-binding site in HSA revealed by our crystallographic studies allows us to design mutagenesis experiments to construct a tailor-made heme pocket for stable O_2 binding. Tyr-161 was the first candidate considered for site-directed mutagenesis to introduce a proximal histidine; however, the Y161H mutation was not done because our simulations indicated that the distance from N_ϵ(H161) to Fe(heme) would be too great (4.0 Å). Instead, modeling experiments suggested that the favorable positions for the axial imidazole insertion would be Ile-142 and Leu-185 (Figure 1). The N_ϵ(histidine)–Fe distances were estimated to be 2.31 Å for H142 and 2.69 Å for H185 (compared to 2.18 Å for Mb). We therefore designed and produced a single mutant I142H and three double mutants I142H/Y161L, I142H/Y161F, and Y161L/L185H (see Experimental Section).

The UV–vis absorption and MCD spectra of the rHSA(I142H/Y161L)–hemin and rHSA(I142H/Y161F)–hemin are

(20) (a) Collman, J. P.; Basolo, F.; Bunnenberg, E.; Collins, T. J.; Dawson, J. H.; Ellis, P. E., Jr.; Marrocco, M. L.; Moscowitz, A.; Sessler, J. L.; Szymanski, T. *J. Am. Chem. Soc.* **1981**, *103*, 5636–5648. (b) Cheek, J.; Dawson, J. H. Magnetic Circular Dichroism Spectroscopy of Heme Proteins and Model Systems. In *The Porphyrin Handbook*; Kadish, K. M., Smith, K. M., Guilard, R., Eds.; Academic Press: San Diego, 2000; Vol. 7, pp 339–369. (c) Svastits, E. W.; Dawson, J. H. *Inorg. Chim. Acta.* **1986**, *123*, 83–86.
(21) Nozawa, T.; Okubo, S.; Hatano, M. *J. Inorg. Biochem.* **1980**, *12*, 253–267.
(22) Monzani, E.; Bonafè, B.; Fallarini, A.; Redaelli, C.; Casella, L.; Minchiotti, L.; Galliano, M. *Biochim. Biophys. Acta* **2001**, *1547*, 302–312.
(23) Geibel, J.; Cannon, J.; Campbell, D.; Traylor, T. G. *J. Am. Chem. Soc.* **1978**, *100*, 3575–3585.
(24) Tolosano, E.; Altruda, F. *DNA Cell Biol.* **2002**, *21*, 297–306.
(25) Paoli, M.; Anderson, B. F.; Baker H. M.; Morgan, W. T.; Smith, A.; Baker, E. N. *Nat. Struct. Biol.* **1999**, *6*, 926–931.

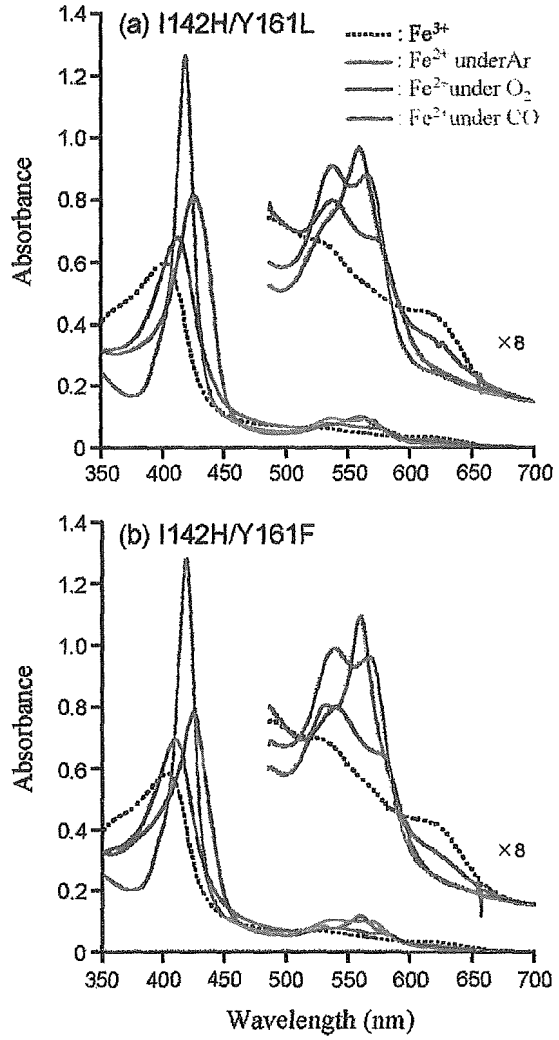

Figure 3. UV-vis absorption spectral changes of the (a) rHSA(I142H/Y161L)-heme and (b) rHSA(I142H/Y161F)-heme in 50 mM potassium phosphate buffered solution (pH 7.0, 8 °C).

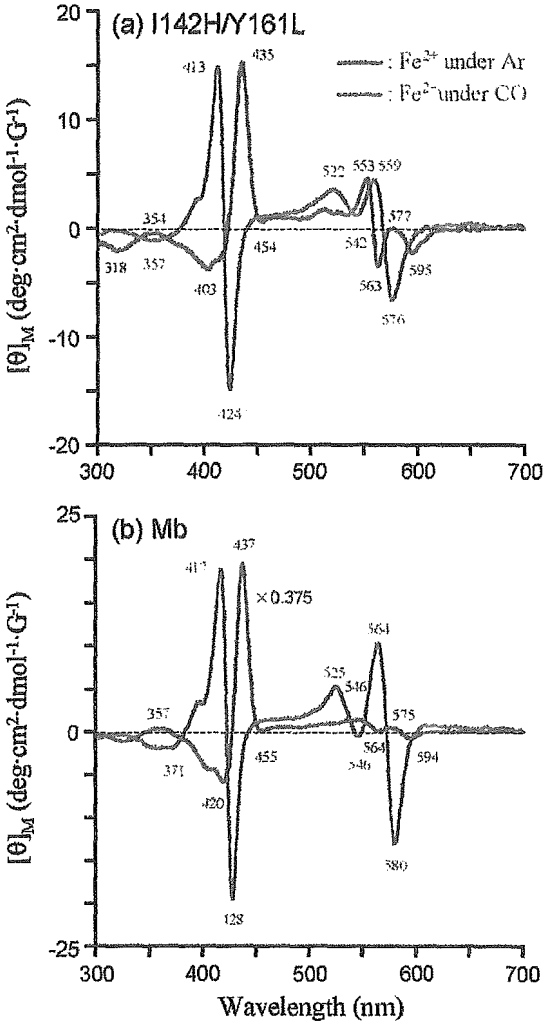

Figure 4. MCD spectral changes of the (a) rHSA(I142H/Y161L)-heme and (b) native Mb in 50 mM potassium phosphate buffered solution (pH 7.0, 22 °C).[30]

essentially the same in their general features (Figure 3 and Figure S2). The strong absorption band due to the porphyrin-to-metal CT was weakened because of the Y161L and Y161F mutations (Figure 3). Both MCD spectra showed similar S-shaped patterns in the Soret band region, which resembled that of ferric Mb (see Figure S2).[26] It is known that two water molecules are located in the heme pocket of ferric Mb.[27] One water axially coordinates to the sixth position of the central ferric ion of the hemin to produce the aquo complex, and the other one is at the rear of the pocket, hydrogen bonded to the first water. A great number of MCD studies on synthetic iron porphyrins and hemoproteins have demonstrated that the spectral shape in the Soret region can be used as a qualitative marker of the spin state and axial coordination environment.[20] Vickery and co-workers found that (i) the Soret MCD intensity of the ferric Mb with different anions at the six-coordinate position was correlated with the amount of low-spin component formed, and (ii) the shape of the band is sensitive to the nature of the sixth ligand.[26] Our MCD results suggest that both the rHSA-(I142H/Y161L)−hemin and rHSA(I142H/Y161F)−hemin are in predominantly ferric high-spin complexes having a water molecule as the sixth ligand.

O_2 and CO Binding to Ferrous rHSA(mutant)−Heme. The rHSA(mutant)−hemin was easily reduced to the ferrous complex by adding a small molar excess of aqueous sodium dithionate under an Ar atmosphere. A single broad absorption band (λ_{max} = 559 nm) in the visible region of the rHSA(I142H/Y161L)−heme and rHSA(I142H/Y161F)−heme was similar to that observed for deoxy Mb[28] or the chelated heme in DMF,[29] indicating the formation of a five-*N*-coordinate high-spin complex (Figure 3, Table 1). The spectral features and amplitude were unaltered in the temperature range of 0−25 °C. The heme therefore appears to be accommodated in the mutated heme pocket with an axial coordination involving His-142. Upon exposure of the rHSA(I142H/Y161L)−heme and rHSA(I142H/

(26) Vickery, L.; Nozawa, T.; Sauer, K. *J. Am. Chem. Soc.* **1976**, *98*, 343−350.
(27) Springer, B. A.; Sligar, S. G.; Olson, J. S.; Phillips, G. N., Jr. *Chem. Rev.* **1994**, *94*, 699−714.
(28) Antonini, E.; Brunori, M. *Hemoglobin and Myoglobin in Their Reactions with Ligands*; North-Holland Pub.: Amsterdam, 1971; p 18.
(29) Traylor, T. G.; Chang, C. K.; Geibel, J.; Berzinis, A.; Mincey, T.; Cannon, J. *J. Am. Chem. Soc.* **1979**, *101*, 6716−6731.

Y161F)–heme solutions to O_2, the UV–vis absorptions immediately changed to that of the O_2 adduct complex at 0–25 °C (Figure 3).[28,29] After flowing CO gas, these hemoproteins produced stable carbonyl complexes.

The MCD spectra of the deoxy and carbonyl rHSA(I142H/Y161L)–heme are shown in Figure 4a. The Soret MCD of the deoxy state under anaerobic conditions is dominated by an intense positive peak at 435 nm, as would be expected for the Faraday *C* terms anticipated for the high-spin Fe^{2+} porphyrin.[20a,26] On the other hand, the rHSA(I142H/Y161L)CO exhibited S-shaped MCDs which correspond to the *A* term bands for the diamagnetic Fe^{2+} porphyrin.[20a,26] These spectra are very similar to those of the high-spin deoxy Mb and low-spin MbCO measured in identical conditions (Figure 4b). Our MCD results clearly show that the central ferrous ion of the heme is coordinated by His-142 in the heme pocket and forms a five-*N*-coordinate high-spin complex under an Ar atmosphere, which converts to the low-spin diamagnetic form by the binding of CO. The rHSA(I142H/Y161F)–heme complex had the same MCD spectral features as rHSA(I142H/Y161L)–heme (data not shown).

The single mutant rHSA(I142H)–heme complex, which retains Y161, could not bind O_2. The polar phenolate residue at the top of the porphyrin plane is likely to accelerate the proton-driven oxidation of the Fe^{2+} center. This rapid autoxidation is also observed in the rMb(H64Y) mutants, in which the distal histidine (His-64) was substituted with Tyr, thus introducing a potentially anionic nucleophile near to the O_2 coordination site.[31] In contrast, replacement of Tyr-161 in rHSA(I142H)–heme by Leu or Phe enhanced the stabilization of the O_2 adduct complex. In the rHSA(Y161L/L185H)–heme, the proximal histidine coordinated to the central ferrous ion from the opposite side of the porphyrin platform also allows O_2 binding to the heme. The lifetimes for the decays of the dioxygenated rHSA(I142H/Y161L)–heme, rHSA(I142H/Y161F)–heme, and rHSA(Y161L/L185H)–heme are all 3–5 min at 20 °C.

To evaluate the kinetics of the O_2 and CO bindings to the rHSA(mutant)–heme, laser flash photolysis experiments were carried out.[14,15] The transient absorption spectra of the photodissociated product of the rHSA(I142H/Y161L)–hemeCO displayed a negative absorbance at 417 nm, due to the disappearance of the carbonyl complex, and a positive absorbance at 435 nm, which is attributed to the deoxy form (Figure 5). The transient absorption spectra in the time range from 0.1 μs to 8.0 ms with an isosbestic point at 401, 426, and 458 nm were superimposed on the static difference spectrum of the deoxy minus carbonyl compound (Figure 5, red line). They illustrate the process of reassociation of CO and are consistent with the formation of the ferrous five-*N*-coordinate high-spin complex after the laser pulse irradiation.

It is noteworthy that the absorbance decays accompanying the CO recombinations to these rHSA(mutant)-heme were composed of double-exponential profiles, which are normally not observed in Mb (Figure 6a). The ratio of the amplitude of the fast and slow phases was approximately 3:2 for the rHSA(I142H/Y161L)-heme, 5:1 for the rHSA(I142H/Y161F)-heme and 3:1 for the rHSA(Y161L/L185H)-heme. On the other hand,

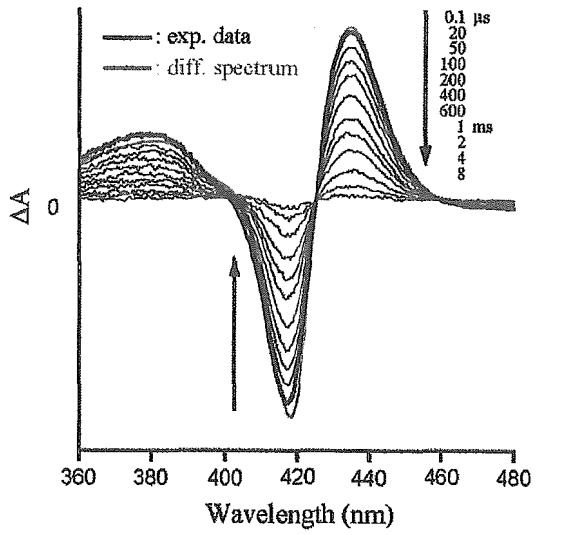

Figure 5. Transient absorption spectra of the photodissociated product of the rHSA(I142H/Y161L)-hemeCO after the laser flash photolysis at 22 °C. The red-line represents the static spectrum of deoxy minus carbonyl compound in Figure 3a.

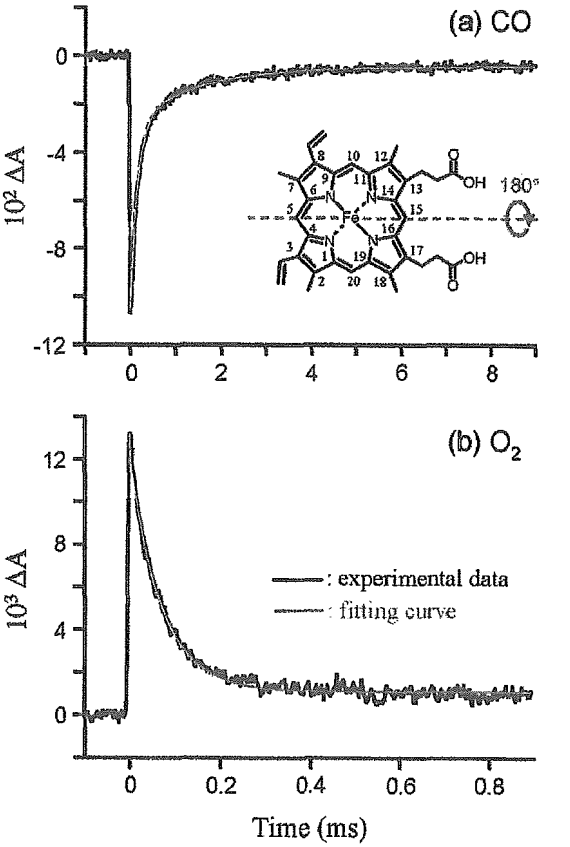

Figure 6. Absorption decay of CO rebinding to the rHSA(I142H/Y161F)-heme after the laser flash photolysis at 22 °C; the kinetics was composed of two phases and relaxation curve was fitted by double-exponentials. (b) Absorption decay of O_2 rebinding to the rHSA(I142H/Y161F)-heme after the laser flash photolysis at 22 °C; the kinetics was fitted by single-exponential relaxation curve.

the rebinding of O_2 to the rHSA(mutant)-heme followed a simple monophasic decay (Figure 6b). From numerous investigations on synthetic model hemes, it has been shown that a bending

(30) The spectra of Mb are consistent with other results reported elsewhere; refs 20, 26.
(31) Springer, B. A.; Egeberg, K. D.; Sliger S. G.; Rohlfs, R. J.; Mathews, A. J.; Olson, J. S. *J. Biol. Chem.* **1989**, *264*, 3057–3060.

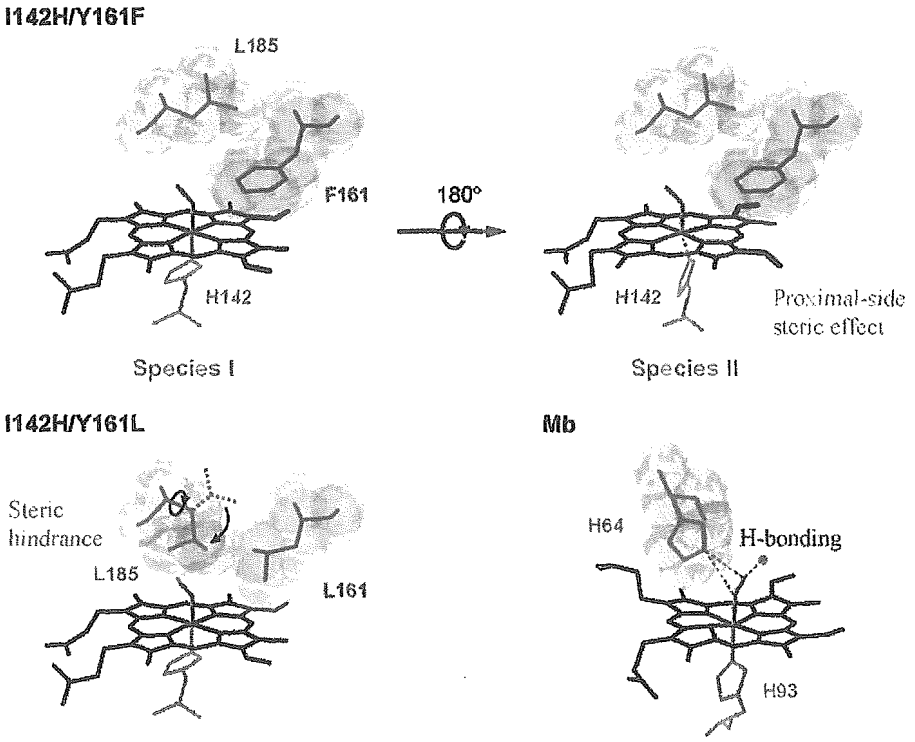

Figure 7. Structural models of the hemeO_2 sites of rHSA(I142H/Y161F)-heme and rHSA(I142L/Y161L)-heme, and comparison to Mb.[12,32]

strain in the proximal base coordination to the central Fe^{2+} atom, the "proximal-side steric effect", can both increase the dissociation rate and decrease the association rate for CO, whereas it increases the O_2 dissociation rate without greatly altering the kinetics of O_2 association.[14,15] One possible explanation is that there may be two different geometries of the axial histidine (His-142 or His-185) coordination to the central ferrous ion of the heme, each one accounting for a component of the biphasic kinetics of CO rebinding. Marden and co-workers also reported a similar two-phase kinetics in CO association with HSA-heme and interpreted it as indicating that there are two different orientations of the porphyrin ring in a single site on HSA.[10] In our case, the alternative geometries may arise because crystallographic analysis suggests that the heme molecule appears able to bind into the narrow cavity of subdomain IB in two orientation that are related by a 2-fold rotation about the 5,15-*meso* axis of the heme (180° rotational isomers). It appears that the asymmetric hydrophobic 3,8-divinyl groups at the porphyrin periphery may occupy different positions that result in a shift of the Fe^{2+} center, forming the two different geometries of the axial imidazole coordination of histidine (Figure 7).

In general, the crystal structures of natural hemoproteins have shown that the prosthetic heme group is bound in a single orientation. On the other hand, in solution, ^{1}H NMR spectra frequently exhibit two sets of heme (or hemin) resonances, which arise from alternative orientations of the porphyrin plane.[33] This orientational disorder is most readily detected in the ferric low-spin state, which shows extraordinary porphyrin 2,7,12,18-CH_3 contact shifts.[34] The amount of the minor species ranges from a few percent in Mb to 40% in insect Hb (*CTT* HbIII).[35] Reconstitution techniques have made significant contributions to clarify this molecular equilibrium; the heme in Hb and Mb can be easily removed under acidic conditions and the resulting apoprotein may be reconstituted by adding back the heme to produce the holoprotein.[36] The incorporation of hemin into apoMb is complete within 1 ms, but the initial complex does not distinguish the two possible orientations of the porphyrin ring.[34] As a result, freshly reconstituted Mb contains an equimolar 1/1 mixture of the two conformers; subsequent heme rearrangement is extremely slow (≈13 h). The influence of the heme orientation on the functional properties appears to be very dependent on the particular protein. In *CTT* HbIII, the O_2 binding affinity depends on the heme orientation.[37] On the other hand, the equilibrium and kinetic parameters for O_2 and CO binding to the reconstituted human Mb are unaffected by the slow heme rearrangement.[38,39]

Our attempts to determine the ratio of the two hemin orientations of the rHSA(I142H/Y161L)-hemin by ^{1}H NMR spectroscopy unfortunately failed. The downfield spectra of the

(32) The model of Mb was prepared on the basis of crystal structure coordinate of MbO_2 (code: 1MBO, Phillips, S. E. *J. Mol. Biol.* **1980**, *142*, 531–554.). The coordinated O_2 shows a hydrogen bond with N_ϵ(His-64) and hydrogen bond network through H_2O (light-blue circle) within the distal pocket.

(33) La Mar, G. N.; Satterlee, J. D.; de Ropp, J. S. Nuclear Magnetic Resonance of Hemoprotein. In *The Porphyrin Handbook*; Kadish, K. M., Smith, K. M., Guilard, R., Eds.; Academic Press: San Diego, 2000; Vol. 5, pp 185–298.

(34) (a) Jue, T.; Krishnamoorthi, R.; La Mar, G. N. *J. Am. Chem. Soc.* **1983**, *105*, 5701–5703. (b) La Mar, G. N.; Toi, H, Krishnamoorthi, R, *J. Am. Chem. Soc.* **1984**, *106*, 6395–6401.

(35) (a) La Mar, G. N.; Davis, N. L.; Parish, D. W.; Smith, K. M. *J. Mol. Biol.* **1983**, *168*, 887–896. (b) La Mar, G. N.; Smith, K. M.; Gersonde, K.; Sick, H.; Overcamp, M. *J. Biol. Chem.* **1980**, *255*, 66–70.

(36) Hayashi, T.; Hisaeda, Y. *Acc. Chem. Res.* **2002**, *35*, 35–43.

(37) Gersonde, K.; Sick, H.; Overkamp, M.; Smith, K. M.; Parish, D. W. *Eur. J. Biochem.* **1986**, *157*, 393–404.

(38) Light, W. R.; Rohlfs, R. J.; Palmer, G.; Olson, J. S. *J. Biol. Chem.* **1987**, *262*, 46–52.

(39) Aojula, H. S.; Wilson, M. T.; Morrison, I. G.*Biochem. J.* **1987**, *243*, 205–210.

Table 2. O_2 Binding Parameters of the rHSA(mutant)-Heme in 50 mM Potassium Phosphate Buffer Solution (pH 7.0) at 22 °C[a]

Hemoproteins	$k_{on}^{O_2}$ ($\mu M^{-1} s^{-1}$)	$k_{off}^{O_2}$ ($m s^{-1}$) I	$k_{off}^{O_2}$ ($m s^{-1}$) II	$P_{1/2}^{O_2}$ (Torr) I	$P_{1/2}^{O_2}$ (Torr) II
rHSA(I142H/Y161L)-Heme	7.5	0.22	1.7	18	134
rHSA(I142H/Y161F)-Heme	20	0.10	0.99	3	31
rHSA(Y161L/L185H)-Heme	31	0.20	2.1	4	41
Hbα (R-state)[b]	33[c]	0.013[d]		0.24	
Mb[e,f]	14	0.012		0.51	
rMb(H64L)[f]	98	4.1		26	
rMb(H64F)[f]	75	10		82	
RBC[g]				8	

[a] Number I or II indicates species I or II. [b] Human Hb α-subunit. [c] In 0.1 M phosphate buffer (pH 7.0, 21.5 °C); ref 40. [d] In 50 mM phosphate buffer (pH 7.0, 20 °C); ref 41. [e] Sperm whale Mb. [f] In 0.1 M potassium phosphate buffer (pH 7.0, 20 °C); ref 16. [g] Human red cell suspension. In isotonic buffer (pH 7.4, 20 °C); ref 42.

Table 3. CO Binding Parameters of the rHSA(mutant)-Heme in 50 mM Potassium Phosphate Buffer Solution (pH 7.0) at 22 °C[a]

Hemoproteins	k_{on}^{CO} ($\mu M^{-1} s^{-1}$) I	k_{on}^{CO} ($\mu M^{-1} s^{-1}$) II	k_{off}^{CO} (s^{-1}) I	k_{off}^{CO} (s^{-1}) II	$P_{1/2}^{CO}$ (Torr) I	$P_{1/2}^{CO}$ (Torr) II
rHSA(I142H/Y161L)-Heme	2.0	0.27	0.013	0.079	0.0053	0.24
rHSA(I142H/Y161F)-Heme	6.8	0.72	0.009	0.061	0.0011	0.068
rHSA(Y161L/L185H)-Heme	3.7	0.35	0.012	0.077	0.0026	0.18
Hbα (R-state)[b]	4.6[c]		0.009[d]		0.0016[e]	
Mb[f,g]	0.51		0.019		0.030	
rMb(H64F)[g]	4.5		0.054		0.0097	

[a] Number I or II indicates species I or II. [b] Human Hb α-subunit. [c] In 50 mM potassium phosphate buffer (pH 7.0, 20 °C); ref 45. [d] In 0.1 M phosphate buffer (pH 7.0, 20 °C); ref 44. [e] Calculated from k_{on}^{CO}/k_{off}^{CO}. [f] Sperm whale Mb. [g] In 0.1 M potassium phosphate buffer (pH 7.0, 20 °C); refs 16, 48.

rHSA(I142H/Y161L)-hemin did not show sharp resonances of the four porphyrin CH_3 groups. Other trials to convert the rHSA-(I142H/Y161L)-hemin in the low-spin azide adduct complex,[33] which is much better suited for the ^1H NMR investigation, also failed even with the addition of a large excess of ligand. In any case, the amplitude ratio of the two phases observed for the CO association to rHSA(mutant)-heme was always the same, independent of time after preparation.

O_2 and CO Binding Parameters. By analyzing the CO/O_2 competitive binding following laser flash photolysis,[14,15] we obtained the association rate constants for O_2 ($k_{on}^{O_2}$) and the O_2 binding affinities [$P_{1/2}^{O_2} = (K^{O_2})^{-1}$] for the rHSA(I142H/Y161L)-heme, rHSA(I142H/Y161F)-heme and rHSA(Y161L/L185H)-heme (Table 2). From eq 6, variation in k_{on}^{CO} arising from the two geometries of the His coordination (the faster phase is defined as species I and the slower phase is defined as species II) yielded two different O_2 binding affinities. In species I, the proximal His may coordinate to the central ferrous ion without strain, whereas in species II, the ligation may involve some distortion, resulting in weaker O_2 binding (Figure 7). The absorbance decay accompanying the CO dissociation from the rHSA(mutant)-hemeCO by the replacement with NO also showed double-exponential profiles, giving two values of k_{off}^{CO} (Table 3). The proximal-side steric effect generally increases the dissociation rate for CO,[14,15] a result that is quite consistent with our interpretation that there are two orientation isomers of the heme (the larger component of k_{off}^{CO} originating from species II).

The $P_{1/2}^{O_2}$ values of the rHSA(mutant)-heme were determined to be 3−18 and 31−134 Torr for species I and II, respectively. Thus even the O_2 binding affinities of species I were 6−75-fold lower than those of native Hbα (R-state) and Mb.[16,40−42] Kinetically, these low affinities for O_2 were due to an 8−18-fold increase in the O_2 dissociation rate constants. Neutron diffraction studies of MbO_2 revealed that there is a direct hydrogen bond between the distal His-64 and the coordinated O_2 (Figure 7).[43] The high-resolution X-ray crystallographic structure of $Hb\alpha O_2$ also suggested a similar interaction in the heme pocket.[44] In both hemoproteins, the distal His stabilizes the bound O_2 by about −1.4 kcal mol^{-1} due to the hydrogen bonding. On the basis of the mutagenesis studies on sperm whale rMb, Rohlfs and co-workers demonstrated that the replacement of His-64 with apolar amino acid residues (Leu or Phe) results in loss of the hydrogen bonding, and markedly increased the O_2 dissociation rates (342−833-fold higher than Mb).[16] In the rHSA(mutant)-heme, the dioxygenated heme is buried in the core of the hydrophobic cavity without any counterpart for the hydrogen bond; thus the even small $k_{off}^{O_2}$ values for species I are greater than those of Hbα and Mb. In species II, the proximal-side steric effect could further increase the dissociation rates and cause a large decline in the O_2 binding affinity. In contrast, the binding parameters of CO to the rHSA(mutant)-heme (species I) exhibited similar values of Hbα (≤3-fold),[45,46] because the coordinated CO in Hbα does not form a hydrogen bond with the distal His-64.[47]

Comparison of the O_2 binding parameters for rHSA(I142H/Y161L)-heme and rHSA(I142H/Y161F)-heme shows that the presence of a Phe rather than Leu at position 161 results in 6-fold and 4-fold increases in the O_2 binding affinity for species I and II, respectively. This is mainly due to an increase in the O_2 association rate constant (Table 2). The same trend was observed for CO binding (3-fold increase in k_{on}^{CO}) (Table 3). The substitution of Leu-161 (102 Å^3) by Phe-161 (137 Å^3)[49] replaces an isopropyl group with a rigid benzyl group within the heme pocket. In I142H/Y161L, the small side-chain of Leu-161 may allow free rotation of the side-chain of neighboring Leu-185, thereby reducing the volume on the distal-side of the porphyrin plane (Figure 7). Actually, modeling and experimental studies suggest that His-185 in Y161L/L185H can coordinate to the central ferrous ion of the heme. On the other hand, the bulkier aromatic side-chain of Phe-161 may prevent rotation of the isopropyl group of Leu-185 and thereby provide greater room of the distal pocket; this might allow easier access to the heme Fe atom and account for the increased association rates for O_2 and CO.

Conclusion

HSA exploits weak axial coordination by Tyr-161 to bind hemin into the heme pocket. Reduction of the central ferric ion partly disrupts the Fe−O(phenolate) bond and produces unusual

(40) Gibson, Q. H. *J. Biol. Chem.* **1970**, *245*, 3285−3288.
(41) Olson, J. S.; Andersen, M. E.; Gibson, Q. H. *J. Biol. Chem.* **1971**, *246*, 5919−5923.
(42) Imai, K.; Morimoto, H.; Kotani, M.; Watari, H.; Hirata, W.; Kuroda, M. *Biochim. Biphys. Acta* **1970**, *200*, 189−197.
(43) Phillips, S. E. V.; Schoenborn, B. P. *Nature* **1981**, *292*, 81−82.
(44) Shaanan, B. *J. Mol. Biol.* **1983**, *171*, 31−59.
(45) Steinmeier, R. C.; Parkhurst, L. J. *Biochemistry* **1975**, *14*, 1564−1571.
(46) Sharma, V. S.; Schmidt, M. R.; Ranney, H. M. *J. Biol. Chem.* **1976**, *251*, 4267−4272.
(47) Hanson, J. C.; Schoenborn, B. P. *J. Mol. Biol.* **1981**, *153*, 117−146.
(48) rMb(H64L) exhibited an abnormally large CO binding affinity and k_{on}^{CO} compared to those of other mutants; ref 16.
(49) Creighton, T. E. *Proteins: Structures and Molecular Properties*; W. H. Freeman and Co.: New York, 1983; p 242.

ferrous four-coordinate intermediate-spin state hemoprotein. We have engineered mutant rHSA-heme complexes which can bind O_2 reversibly with an affinity that is only 1 order of magnitude lower than the affinity of O_2 for Hbα (R-state) and Mb. The principal modifications to the heme pocket that are required to confer reversible O_2 binding are (1) replacement of Tyr-161, the endogenous anionic nucleophile, by hydrophobic amino acid (Leu or Phe), and (2) introduction of His as a proximal base at position Ile-142 or Leu-185 (either side of the porphyrin ring plane). The transport of O_2 by the rHSA-heme could be of tremendous clinical importance not only as a red cell substitute but also as an O_2-providing therapeutic reagent. Although a number of Hb-based O_2 carriers have already been developed, the administration of these materials often elicits an acute increase in blood pressure by vasoconstriction.[50-52] This side-effect is caused by the rapid capture of the endothelial-derived relaxing factor, namely NO, by Hb that has leaked through the vascular endothelium. In contrast, our rHSA(mutant)-heme would not induce such hypertension, because the albumin carrier has low permeability through the muscle capillary pore.[53]

Our results on several mutants have also shown that modification of the distal-side of the heme pocket has a measurable effect on O_2 binding affinity (compare Leu-161 and Phe-161). To develop this promising O_2 carrier as a blood substitute, further work using a combined mutagenic and synthetic approach is required; (1) additional mutations, e.g. an introduction of a distal base which in Mb and Hbα forms a hydrogen bond with the coordinated O_2, may help to stabilize the O_2 adduct complex, and (2) small modifications to the heme structure designed to adjust its position within the pocket interior but without straining the proximal His coordination, may improve and modulate the O_2 binding ability. To aid these modifications, crystal structural analysis of rHSA(mutant)-heme complexes is now underway.

Acknowledgment. This work was supported by a Grant-in-Aid for Scientific Research (No. 16350093) from JSPS, a Grant-in-Aid for Exploratory Research (No. 16655049) from MEXT Japan, Health Science Research Grants (Regulatory Science) from MHLW Japan, and Wellcome Trust (UK). The work at Imperial College London was partially carried out as the Japan-UK Research Cooperative Program (Joint Project) of JSPS.

Supporting Information Available: UV−vis absorption and MCD spectra of FePPIXDME, MCD spectra of the ferric rHSA-(mutant)-hemin and aquo-metMb. This material is available free of charge via the Internet at http://pubs.acs.org.

JA054819U

(50) Tsuchida, E. Perspectives of Blood Substitutes. In *Blood Substitutes: Present and Future Perspectives*; Tsuchida, E., Ed.; Elsevier Science: Lausanne, 1998; pp 1−14.
(51) Winslow, R. M. *Annu. Rev. Med.* **1999**, *50*, 337−353.
(52) Squires, J. E. *Science* **2002**, *295*, 1002−1005.
(53) Tsuchida, E.; Komatsu, T.; Matsukawa, Y.; Nakagawa, A.; Sakai, H.; Kobayashi, K.; Suematsu, M. *J. Biomed. Mater. Res.* **2003**, *64A*, 257−261.

Albumin Clusters: Structurally Defined Protein Tetramer and Oxygen Carrier Including Thirty-Two Iron(II) Porphyrins

Teruyuki Komatsu,* Yukiko Oguro, Akito Nakagawa, and Eishun Tsuchida*

Advanced Research Institute for Science and Engineering, Waseda University, 3-4-1 Okubo,Shinjuku-ku, Tokyo 169-8555, Japan

Received June 30, 2005; Revised Manuscript Received August 10, 2005

Recombinant human serum albumin (rHSA) clusters have been synthesized and physicochemically characterized. Cross-linking between the Lys groups of the core albumin and a unique Cys-34 of the shell albumins with an *N*-succinimidyl-6-[3′-(2-pyridyldithio)propionamido]hexanoate produced the structurally defined rHSA trimer and tetramer. MALDI-TOF−MS showed a single peak with the triple and quadruple masses of rHSA. Their molar ellipticities and the isoelectric points (p*I* = 4.8) are all identical to those of the monomer, suggesting that the essential structures of the albumin units were intact. TEM observations demonstrated a uniform morphology of the rHSA tetramer with a diameter of 20−30 nm. The circulation half-life ($\tau_{1/2}$) of the ^{125}I-labeled rHSA tetramer in rat (5.5 h) was significantly longer than that of the monomer (2.3 h) due to the low ratio of the distribution phase (α-phase). A total of 24 and 32 molecules of the synthetic iron(II) porphyrins (FePs) are incorporated into the hydrophobic cavities of the rHSA trimer and tetramer, respectively, producing huge artificial hemoproteins. These albumin−heme clusters can reversibly bind and release O_2 under physiological conditions (37 °C, pH 7.3) and showed similar O_2-binding properties (O_2-binding affinity, association and dissociation rate constants) to those of the corresponding monomer. A large volume of O_2 can be chemically dissolved into the albumin−heme cluster solutions relative to the monomeric rHSA-FeP when the molar concentration of the albumin scaffold is identical.

Introduction

In our bloodstream, hydrophobic molecules of medium size (ex., long-chain fatty acids, bilirubin, steroids, hemin) are captured by human serum albumin (HSA, Mw: 66.5 kDa) and are allowed to circulate for a relatively long time to reach the disposal sites in the body.[1] The transporting ability of this shuttle protein contributes to maintaining the high concentration levels of the therapeutic drugs in the circulatory system.[1,2] Moreover, the albumin peptide exhibited a slow terminal clearance and catabolism, so that the conjugation of HSA with a therapeutic protein (ex., soluble CD4 and interferon-α) provides clinical benefits in permitting less frequent administrations.[3] We have found that synthetic iron(II) porphyrins (hemes) were incorporated into the hydrophobic cavities of HSA, producing an albumin−heme hybrid, which can reversibly bind and release dioxygen (O_2) under physiological conditions (pH 7.3, 37 °C).[4] This artificial hemoprotein has the capability to carry O_2 like hemoglobin (Hb) or myoglobin (Mb) and functions as a red blood cell (RBC) substitute in vivo.[5]

One of the interesting characteristics of the HSA structure is the presence of a single reactive thiol of Cys-34.[1,6] The reaction of the bifunctional reagent, 1,6-bis(maleimido)-hexane (BMH), with HSA successfully creates an intermolecular covalent bridge between the two Cys-34s.[7] A total of 16 molecules of synthetic heme were accommodated into the dimer and the obtained albumin−heme dimer solution is able to transport a large volume of O_2 compared to the human blood ([heme] = 9.2 mM) while maintaining the colloid osmotic pressure on a physiological level.[7b] Another remarkable advantage of the HSA dimer is its long circulation persistence relative to the monomer, since the 2× size of the molecule could serve to remain in the blood vessel. We now extend this approach to produce the structurally defined albumin trimer and tetramer, namely "albumin clusters". In this paper, we report, for the first time, the synthesis, physicochemical characterization, and preliminary pharmacokinetics of the albumin clusters cross-linked by *N*-succinimidyl-6-[3′-(2-pyridyldithio)propionamido]hexanoate (SPDPH), which efficiently connects an NH_2 group of Lys and an SH group of Cys. The O_2-binding properties of the albumin−heme clusters incorporating the 2-[8-{*N*-(2-methylimidazolyl)}octanoyloxymethyl]-5,10,15,20-tetrakis{α,α,α,α-*o*-(1-methylcyclohexanamido)phenyl}porphinatoiron(II) (FeP, Scheme 1), are also evaluated and compared to those of the corresponding monomer.

Experimental Section

Materials and Apparatus. An rHSA (Albrec, 25 wt %) was provided from the NIPRO Corp (Osaka, Japan). Ethanol, dithiothreitol, and 2,2′-dithiopyridine (all high-purity grades) were purchased from Kanto Chemical Co., Inc. (Tokyo) and used without further purification. *N*-Succinimidyl-6-[3′-(2-pyridyldithio)propionamido]hexanoate (SPDPH) was

* To whom correspondence should be addressed. Prof. Eishun Tsuchida, Ph.D. Tel: +81-3-5286-3120. Fax: +81-3-3205-4740. E-mail: eishun@waseda.jp (Eishun Tsuchida). E-mail: teruyuki@waseda.jp (Teruyuki Komatsu).

10.1021/bm050454u CCC: $30.25
Published on Web 10/13/2005

Scheme 1

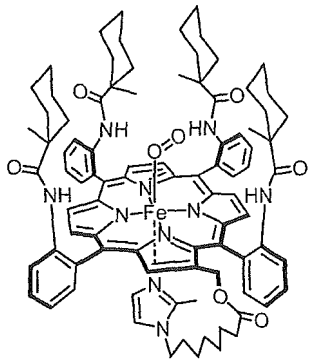

purchased from Pierce Biotechnology (Rockford, USA). 2-[8-{*N*-(2-Methylimidazolyl)}octanoyloxymethyl]-5,10,15,20-tetrakis{α,α,α,α-*o*-(1-methylcyclohexanamido)-phenyl}porphinatoiron(II) (FeP) was prepared according to our previously reported procedure.[8]

Synthesis of rHSA Clusters. Ethanolic SPDPH (20 mM, 0.75 mL) was slowly added dropwise into the rHSA solution (0.75 mM, 2.0 mL) and gently stirred for 20 min at room temperature. The reaction mixture was diluted with phosphate-buffered saline (PBS, 10 mM, pH 7.4, 25 mL) and concentrated to 2.5 mL using an ADVANTEC UHP-76K ultrafiltration system with a Q0500 076E membrane (cutoff Mw 50 kDa). This washing was repeated three times to remove the excess SPDPH, affording 3′-(2-pyridyldithio)propionamido]hexanoated albumin (PDPH−rHSA, [rHSA] = 5.15 wt %, 2 mL). The albumin concentrations were normally measured by bromcresol green (BCG) methods using a Wako AlbuminB−Test.[9] The number of PDPH chains introduced into rHSA was determined by the assay of 2-thiopyridinone (2TP) with an absorption at 343 nm [molar absorption coefficient (ϵ_{343}): 8.1×10^3 $M^{-1}cm^{-1}$]. A 15-fold molar excess of dithiothreitol (DTT, 1 M, 1.35 μL) was added to the PBS solution of PDPH−rHSA (30 μM), and the formed 2-TP was quantitatively assayed after 10 min.

On the other hand, aqueous DTT (1.0 M, 56 μL) was added to the phosphate-buffered solution (pH 7.0, 10 mM) of rHSA (0.75 mM, 20 mL), and the solution was quickly mixed by a vortex mixer, followed by incubation for 30 min at room temperature. The resultant was washed three times with PBS the same as above, yielding a mercapto−albumin (SH−rHSA, 13 mL, [rHSA] = 7.77 wt %). The mercapto ratio of the Cys-34 was confirmed as 100% using the 2,2′-ditiopyridine (2,2′-DTP) procedure.[10,11]

The SH−rHSA solution was then added to the PDPH−rHSA, and the mixture was gently stirred for 20 h at room temperature. The Native-PAGEs were performed using an Amersham Biosciences Electrophoresis Power Supply EPS 301 with a PAG Mini Daiichi 2/15 (Daiichi Pure Chemicals, Co. Ltd.). The Native-PAGE pattern of the obtained reactant showed six bands including the unreacted SH−rHSA monomer. The HPLC measurement also demonstrated the formation of the rHSA clusters with a high molecular weight. The HPLC system consisted of a Shimadzu LC-8A pump and a Shimadzu SPD-10A UV detector. A Shodex Protein KW-803 column was used with PBS (pH 7.4) as the mobile phase at 25 °C (1.0 mL min^{-1}). Peak fitting of the elution curve was done using a Hulinks PeakFit program.

The rHSA clusters were purified by gel column chromatography using a BIO-RAD EGP Combo Rec system with Superdex 200pg (Pharmacia Corp., 5 cmϕ × 40 cm) and PBS (pH 7.4) as the mobile phase (3.5 mL min^{-1}). The eluant was monitored at 280 nm and fractionated by a BIO-RAD model 2110 collector. The fraction showing the single bands for band C and D in the Native-PAGE was then carefully collected. The matrix associated laser desorption ionization time-of-flight mass spectra (MALDI-TOF−MS) were obtained using a Shimadzu AXIMA-CFR Kompact MALDI. The 10 mg mL^{-1} sinapinic acid in 40% aqueous CH_3CN was used as a matrix. The purity of the each component was checked by the HPLC measurement. The obtained yield was 10% for the rHSA trimer (band C) and 7% for the rHSA tetramer (band D).

Physicochemical Properties. The UV−vis absorption spectra were recorded on a JASCO V-570 spectrophotometer. The measurements were normally performed at 25 °C. Circular dichroism (CD) spectra were obtained using a JASCO J-725 spectropolarimeter. The concentration of the rHSA sample was 2 μM in PBS, and quartz cuvettes with a 1.0-mm thickness were used for the measurements over the range of 195−250 nm.

Transmission Electron Microscopy (TEM). An aqueous solution of the albumin cluster was mixed with 2% phosphotungstic acid (pH 7), and the droplet was placed onto a 200 mesh carbon-coated copper grid, which was hydrophilized by a JEOL HDT-400 hydrophilic treatment device prior to use. The grid was allowed to air-dry and observed in a JEOL JEM-1011 electron microscope at an accelerating voltage of 100 kV.

Circulation Lifetime in Vivo. The 125-Iodinated rHSA tetramer was prepared by our previously reported procedures.[7b] The recovered ^{125}I-albumin had a specific activity of 24.3 MBq mg^{-1} and was diluted by nonlabeled albumin tetramer before administration into anesthetized Wistar rats (ca. 250 g, male). The kinetics of the albumin clearance from the circulation was monitored by measuring the radioactivity in the plasma phase of blood taken from the lateral tail veins using an Aloka ARC 2000 Autowell Gamma Counter. Acid precipitability of the recovered radioactivity was confirmed by the TCA method.[7b,12] The rats were sacrified 8 days after the sample injection by hemorrhage. The radioactivity of the excised organs was also measured. The care and handling of the animals were in accordance with NIH guidelines.

Preparation of Albumin−Heme Clusters. The preparations of albumin−heme clusters (rHSA−FeP trimer and tetramer) were carried out by mixing the EtOH solution of carbonyl−FeP and an aqueous phosphate-buffered solution of albumin clusters according to our previously reported procedures ([FeP]/[rHSA] = 26/1 or 34/1 (mol/mol)).[4a,7b,8] The albumin concentrations were measured using the CD spectra, and the amount of FeP was determined by the assay of the iron ion concentration using inductively coupled plasma spectrometry (ICP) with a Seiko Instruments SPS 7000A spectrometer.

Magnetic Circular Dichroism (MCD). MCD spectra for the phosphate-buffered solution of the albumin–heme clusters (10 μM) under N_2, CO, and O_2 atmospheres were measured using a JASCO J-820 circular dichrometer fitted with a 1.5 T electromagnet. The CD spectra at 0 T were always used as a baseline for each condition.

O_2-Binding Equilibrium and Kinetics. O_2 binding to FeP was expressed by eq 1:

$$\mathrm{FeP} + \mathrm{O_2} \underset{k_{off}}{\overset{k_{on}}{\rightleftharpoons}} \mathrm{FeP(O_2)} \qquad (K = k_{on}/k_{off}) \qquad (1)$$

The O_2-binding affinity (gaseous pressure at half O_2 binding for heme, $P_{1/2} = 1/K$) was determined by UV–vis absorption spectral changes at various O_2 partial pressure.[4b,8,13] The appropriate O_2/N_2 gas mixture (Po_2: 0, 10, 20, 30, 80, 160, and 760 Torr) was prepared by a KOFLOC Gasblender GB-3C, and each spectrum was measured after flowing the gas for 15 min at 25 or 37 °C. FeP concentrations of 20 μM were normally used for the measurements in the range of 350–700 nm. The O_2-binding constant (K) was then calculated from the difference of the absorbance at 444 nm using Drago's equation.[4b,8] The half-lifetimes of the dioxygenated species of the albumin–heme clusters were determined by the time dependence of the absorption intensity for the O_2–adduct complex (549 nm).

The association and dissociation rate constants for O_2 (k_{on} and k_{off}) were measured by a competitive rebinding technique using a Unisoku TSP-1000WK–WIN time-resolved spectrophotometer with a Spectron Laser Systems SL803G-10 Q-switched Nd:YAG laser, which generated a second-harmonic (532 nm) pulse of 6-ns duration (10 Hz). A 150 W xenon arc-lamp was used as the monitor light source. The concentration of the albumin–heme cluster was normally 20 μM and experiments were carried out at 25 °C. The absorption decays accompanying the O_2 association obeyed three-component kinetics. We employed triple-exponentials equation to analyze the absorption decays; $\Delta A(t)$[4c]

$$\Delta A(t) = \mathrm{C_1}\exp(-k_1 t) + \mathrm{C_2}\exp(-k_2 t) + \mathrm{C_3}\exp(-k_3 t) \quad (2)$$

where k_1, k_2, and k_3 are apparent rate constants for the each components.

O_2-Concentration Measurements. The chemically dissolved O_2 in albumin–heme cluster solution was measured using an Ocean Photonics FOXY2000 Fiber Optic Oxygen Sensor with a USB2000 multichannels monochromator and FOXY-AL300 fiber optic sensor (Tokyo). This apparatus uses the fluorescence of a ruthenium complex to measure the partial pressure of O_2. The addition of 0.1 mL of CO to the phosphate-buffered solution of the dioxygenated rHSA–FeP cluster or monomer ([FeP]: 50 μM, 2.0 mL, [O_2]: 700 Torr) in the closed tube immediately dissociates the coordinated O_2 from FeP and increases the dissolved O_2 content in the aqueous phase.

Results and Discussion

Synthesis and Characterization of rHSA Clusters. We have shown that covalent cross-linking a unique Cys-34 of rHSA with BMH provided a defined rHSA dimer, in which

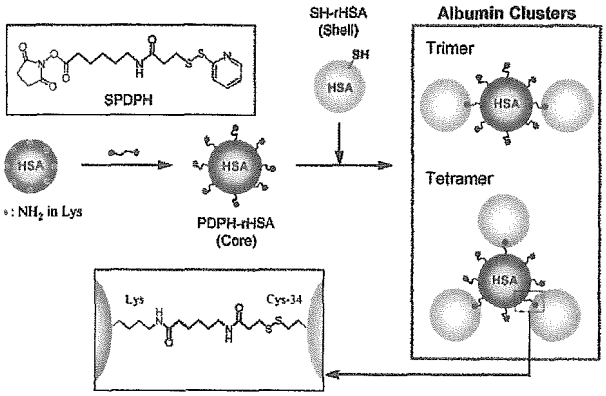

Figure 1. Synthetic scheme of albumin clusters with SPDPH.

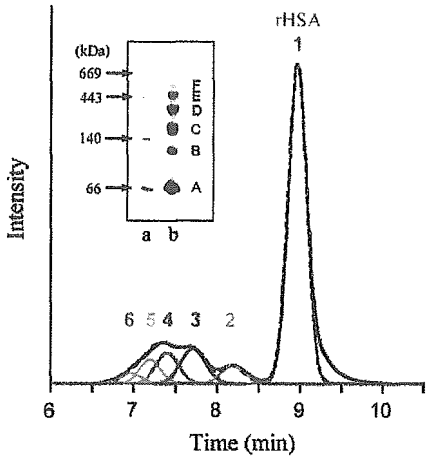

Figure 2. Native-PAGE electrophoresis and HPLC elution curve of the reaction mixture at 25 °C. In the Native-PAGE pattern, lane a, protein ladder; lane b, the reaction mixture (band A: rHSA monomer). The HPLC profile was simulated by a six-components model using a PeakFit (the dotted line, the sum of the simulated six components; peak 1, rHSA monomer).

the essential structures of the rHSA unit are intact.[7b] We now extend this approach to produce albumin clusters. Our first attempt to connect the Cys-34 of rHSAs by multi-armed maleimido(polyoxyethylene) unfortunately failed. The maleimido-terminate at the polyoxyethylene chains are likely to be too flexible to react with the small thiol on the large rHSA molecule to make albumin clusters. On the other hand, *N*-succinimidyl-6-[3′-(2-pyridyldithio)propionamido]hexanoate (SPDPH) was successfully connected to an NH_2 group of Lys and an SH group of Cys on the protein surface. Since rHSA contains 59 Lys in the globular structure, mixing a small molar excess SPDPH with rHSA immediately produced a 6-[3′-(2-pyridyldithio)propionamido]hexanoated rHSA (PDPH–rHSA; Figure 1). Assay of the pyridyldithio residues revealed that approximately 8.3 chains of PDPH were introduced into one rHSA molecule. The PDPH–rHSA acts as a core albumin for the next reaction.

Dithiothreitol (DTT) selectively reduces the mixed-disulfide of Cys-34[10,11] producing a mercapto–rHSA (SH–rHSA) as a shell albumin. After removing DTT, SH–rHSA was slowly dropwise added to the PDPH–rHSA and stirred for 20 h at room temperature (Figure 1). Native-PAGE of the reactant showed six distinct migration bands (Figure 2 inset, lane b: A–F, band A: SH–rHSA). On the basis of the

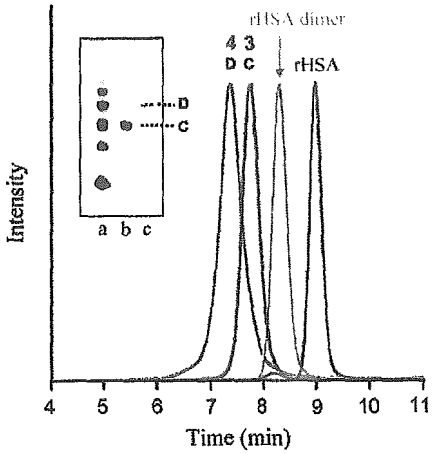

Figure 3. Native-PAGE electrophoresis and HPLC elution curves of the isolated rHSA clusters at 25 °C. In the Native-PAGE pattern, lane a, reaction mixture before purification; lane b, isolated band C; lane c, isolated band D. In the HPLC profiles, red line, rHSA monomer; orange line, rHSA dimer bridged through Cys-34 by BMH; blue line, isolated band C, which corresponds to the rHSA trimer; green line, isolated band D, which corresponds to the rHSA tetramer.

Table 1. Molecular Masses and *pI* Values of rHSA Monomer, Dimer, and Clusters

	M_w		
	obs.[a]	calcd.	*pI*
rHSA[b]	66331	66451	4.8
rHSA dimer[b,c]	132 741	133 180	4.8
band C (rHSA trimer)	200 469	201 614	4.8
band D (rHSA tetramer)	266 538	267 953	4.8

[a] Measured by MALDI-TOF–MS. [b] From ref 7b. [c] rHSA dimer bridged Cys-34 by BMH.

comparison with the protein ladder (lane a), the molecular weights of the bands B, C, and D were estimated to be ca. 130, 200, and 260 kDa, respectively. It can be postulated that they are the rHSA dimer, trimer, and tetramer. The pyridylditio terminates of the core albumin reacted with the single active Cys-34 of the shell albumin creating albumin clusters. The HPLC profile of the reaction mixture exhibited broad multiple bands in the range of 6.5–8.5 min before the rHSA peak (9.0 min; Figure 2). From the careful inspection of the elution curve by peak fitting simulation, we could divide the entire pattern into six components (peaks 1–6). Most probably, the peaks 2–6 correspond to the rHSA dimer to hexamer. Gel permeation chromatography also showed a similar elution curve. Several synthesis repetitions always gave the same patterns in Native-PAGE, HPLC, and GPC. The fractions whose Native-PAGE showed bands C and D were then corrected (Figure 3, inset lanes b and c). Their HPLC profiles exhibited a sharp peak at the exactly the same position where we predicted for peaks 3 and 4 in Figure 2.

The MALDI-TOF–MS of the components of peaks 3 (band C) and 4 (band D) showed a molecular masses at *m/z* 200 469 and 266 538, respectively, which are in good agreement with the calculated value of the rHSA trimer and tetramer (M_w = 201 614 and 267 953) within a difference of 0.5% (Table 1). We first isolated the well-defined rHSA trimer and tetramer in which the Lys groups of the core

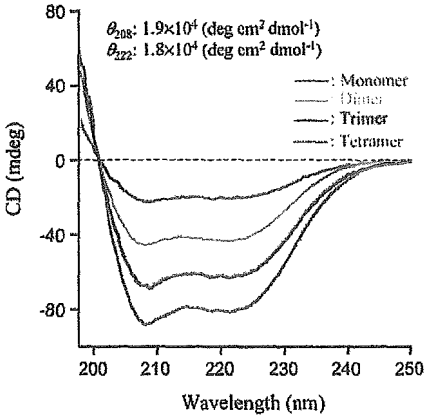

Figure 4. CD spectra of rHSA monomer, dimer bridged through Cys-34 by BMH and clusters in PBS solution (pH 7.4) at 25 °C.

albumin are covalently bridged by the Cys-34 group of the shell albumins.

The peak area evaluations for the six components in Figure 2 indicated their molar ratios in the reaction mixture; monomer (88.2%), dimer (3.1%), trimer (4.3%), tetramer (2.5%), pentamer (1.4%), and hexamer (0.5%). Because the average degree of polymerization was 3.3, we estimated the reaction ratio (X) of the PDPH–rHSA

$$\text{reacted PDPH–rHSA:unreacted (PDPH–rHSA + SH–rHSA)} = X:(1 - X) + (10 - 2.3X) = 11.8:88.2 \quad (3)$$

Thus, X was calculated to be 1.0; this means that all of the PDPH–rHSA (core albumin) participated in the reaction with the shell albumin. The formation ratio of each cluster can be estimated; dimer (26%), trimer (36%), tetramer (22%), pentamer (12%), and hexamer (4%).

The CD spectral patterns (λ_{min} = 208 and 222 nm) and the molar ellipticities at 208 and 222 nm ($[\theta]_{208} = 1.9 \times 10^4$ deg cm^2 dmol^{-1}, $[\theta]_{222} = 1.8 \times 10^4$ deg cm^2 dmol^{-1}) of the isolated rHSA trimer and tetramer were identical to those of the monomer and dimer (Figure 4).[4b,7b] Their isoelectric points (pI = 4.8) were also identical to that of rHSA (Table 1). These results implied that the secondary/tertiary structure, the α-helix content, and surface net charges of the rHSA units were intact after the cluster formation.

TEM of the negatively stained samples of the rHSA tetramer showed homogeneous particles with a diameter of 20–30 nm (Figure 5a,b). The appearance of the cluster solutions was unchanged for over one year and underwent no aggregation and precipitation. We postulate that one tetramer consists of four rHSA molecules bound in the trigonal pyramid form, which was drawn as a model in Figure 5c. rHSA involves a total of 59 Lys groups, and the cross-linker SPDPH can statistically bind to the surface. On the basis of the assay of the dithiopyridyl group, we found that the 8.3 functional PDPH arms are introduced into the core albumin. The shell albumins (SH–rHSAs) therefore approach the PDPH–rHSA from all directions to form a disulfide bridge with Cys-34. As a consequence, the conformation of the tetramer should become a trigonal pyramid-like structure, which is the most favorable arrangement to avoid the steric repulsion of the albumin units.